Journal of Computational Neuroscience 8, 251–273 (2000)

A Model Study of Cellular Short-Term Memory Produced by Slowly Inactivating Potassium Conductances

B. DELORD, P. BARADUC, R. COSTALAT, Y. BURNOD AND E. GUIGON
INSERM U483, Université Pierre et Marie Curie, 9, quai Saint-Bernard, 75005 Paris, France
guigon@ccr.jussieu.fr

Received January 11, 1999; Revised April 23, 1999; Accepted June 16, 1999

Action Editor: Charles Wilson

Abstract. We analyzed the cellular short-term memory effects induced by a slowly inactivating potassium (Ks) conductance using a biophysical model of a neuron. We first described latency-to-first-spike and temporal changes in firing frequency as a function of parameters of the model, injected current and prior history of the neuron (deinactivation level) under current clamp. This provided a complete set of properties describing the Ks conductance in a neuron. We then showed that the action of the Ks conductance is not generally appropriate for controlling latency-to-first-spike under random synaptic stimulation. However, reliable latencies were found when neuronal population computation was used. Ks inactivation was found to control the rate of convergence to steady-state discharge behavior and to allow frequency to increase at variable rates in sets of synaptically connected neurons. These results suggest that inactivation of the Ks conductance can have a reliable influence on the behavior of neuronal populations under real physiological conditions.

Keywords: cellular short-term memory, inactivation, potassium conductance, biophysical model

Introduction

The temporal behavior of biological neural networks depends on interaction between the intrinsic properties of single neurons and synaptic connections between neurons (Llinás, 1988; Harris-Warrick and Marder, 1991; Bargas and Galarraga, 1995; Marder et al., 1996). A great variety of endogenous neuronal dynamics shape the output of neural networks. Rhythmic bursting, plateau potentials, and postinhibitory rebound are crucial in the central pattern generator networks of invertebrates (Harris-Warrick and Marder, 1991). Intrinsic membrane oscillations could be involved in the generation of synchronous firing of large neuronal populations in vertebrates (Llinás, 1988; Silva et al., 1991). There is evidence that spike-frequency adaptation due to calcium-gated potassium conductances modulates gain in neuronal feedback systems (Lisberger and Sejnowski, 1992) and determines the temporal complexity and dynamics of how representations are recalled in associative memory networks (Cartling, 1993; Barkai et al., 1994; Cartling, 1997). Short-lasting synaptic inputs may be transformed into long-lasting motor output in motoneurons (Kiehn, 1991; Booth et al., 1997) and sustained discharges maintained in prefrontal neurons (Guigon et al., 1995; Delord et al., 1997; Camperi and Wang, 1998) by a property of bistability.

Cellular forms of short-term memory induced by low-threshold slowly inactivating outward conductances are ubiquitous and widely recognized intrinsic properties of neurons (the generic term Ks is used to indicate these conductances in this text) (Byrne et al., 1979; Byrne, 1980; Getting, 1983; Storm, 1988; Bargas et al., 1989; Huguenard and Prince, 1991; Spain et al., 1991a; Hammond and Crépel, 1992; Marom

and Abbott, 1994; Nisenbaum et al., 1994; Wang and McKinnon, 1995; Turrigiano et al., 1996; Gabel and Nisenbaum, 1998). The most striking effect of these conductances is to prolong the latency-to-first-spike ($\sim$0.1 to 10 s) in response to current steps (Storm, 1988; Turrigiano et al., 1996). This property is due to a *memory of inhibition*: hyperpolarization of the neuron deinactivates the conductance and slows down the rate of membrane potential change during a subsequent depolarization (Storm, 1988). Some neurons also display a *memory of excitation*: a period of depolarization inactivates the conductance and increases the response of the neuron to subsequent inputs (Turrigiano et al., 1996).

The existence of such forms of memory has led to the suggestion that the Ks conductances contribute to the temporal integration of synaptic inputs (Storm, 1988; Hammond and Crépel, 1992; Surmeier et al., 1991; Nisenbaum et al., 1994; Gabel and Nisenbaum, 1998) and to the patterning of discharge (Getting, 1983; Hammond and Crépel, 1992; Nisenbaum et al., 1994; Gabel and Nisenbaum, 1998), by controlling the latency of the first spike (Storm, 1988; Bargas et al., 1989; McCormick, 1991; Lüthi et al., 1996; Turrigiano et al., 1996) and repetitive firing (Surmeier et al., 1991; Hammond and Crépel, 1992). More generally these cellular computations could contribute to dynamics and operation of neural networks, such as coding by the time of the spike and processing sequential information.

However, it is necessary to examine the conditions under which cellular short-term memory may exist and the strength of these effects before considering these promising computational functions. Most studies of Ks conductances have been performed *in vitro* using constant or ramp stimulating currents, whereas neurons *in vivo* receive widely fluctuating synaptic inputs (Shadlen and Newsome, 1994). This study was therefore carried out to describe the actions of a Ks conductance under current clamp (*in vitro*) and under random synaptic stimulations *in vivo* in a biophysical model of a neuron. We have specifically examined how the memory of inhibition induced by this conductance is expressed under these conditions. We first evaluated the discharge behavior of the model under current clamp protocols (*in vitro* conditions). Several models have examined the effects of Ks conductance inactivation on latency-to-first-spike (Marom and Abbott, 1994; Rush and Rinzel, 1995), oscillatory properties of discharge (Wang, 1993; Rush and Rinzel, 1995), and synaptic transmission in dendrites (Wilson, 1995). However, no one model has systematically documented the discharge latency and frequency effects that result from the presence of a Ks conductance. We have developed a simplified analytical description that clarifies the influence of the Ks conductance on the discharge of the neuron. The second part investigates the properties of the same model under synaptic stimulation by stochastic Poisson inputs and within neuronal networks.

Methods

An isopotential model was used to evaluate the effect of a slowly-inactivating potassium (Ks) conductance on the discharge behavior of a neuron. The model is not meant to represent a particular neuron but rather to describe the typical influence of the conductance on somatic spiking processes. However, the model was based as much as possible on data from a single type of neuron (neocortical pyramidal neuron) to study the conductance in a coherent physiological context. The model comprised four conductances: the sodium and potassium conductances of the action potential (Na, K), a leakage conductance (leak), and the Ks conductance. The discharge behavior of the model neuron was assessed using two stimulation protocols (*in vitro*, *in vivo*).

Isopotential Neuron Model

The change in the membrane potential was given by the following equation:

$$C\frac{dV}{dt} + I_{Na} + I_K + I_{Ks} + I_{leak} - I = 0,$$

where the membrane capacitance C is 1 μF.cm^{-2}. The leakage current was given by $I_{leak} = g_{leak}(V - E_{leak})$, where $E_{leak} = -70$ mV and $g_{leak} = 0.05$ mS.cm^{-2} (passive time constant $\tau = 20$ ms). The current I was either the injected current (*in vitro* conditions) or the synaptic current (*in vivo* conditions). A positive injected current was depolarizing.

Action Potential Conductances

The models of action potential conductances were derived from Lytton and Sejnowski (1991). The fast sodium current was described by

$$I_{Na} = \bar{g}_{Na} m_\infty^3 h(V - E_{Na}),$$

where $E_{Na} = 45$ mV and $\bar{g}_{Na} = 20$ mS.cm^{-2}. The activation gate m was replaced by its steady state activation function, with

$$\alpha_m(V) = \frac{0.55(V + 45.5)}{1 - \exp\left(\frac{-V-45.5}{4}\right)}$$

$$\beta_m(V) = \frac{0.44(V + 18.5)}{\exp\left(\frac{V+18.5}{5}\right) - 1}.$$

The inactivation gate followed first-order kinetics with

$$\alpha_h(V) = 0.115 \exp\left(\frac{-V - 48}{18}\right)$$

$$\beta_h(V) = \frac{3.6}{1 + \exp\left(\frac{-V-25}{5}\right)}.$$

The fast potassium current was given by

$$I_K = \bar{g}_K n^4 (V - E_K),$$

where $E_K = -85$ mV and $\bar{g}_K = 1.5$ mS.cm^{-2}. The kinetics of n followed

$$\alpha_n(V) = \frac{0.0178(-V - 50)}{\exp\left(\frac{-V-50}{5}\right) - 1}$$

$$\beta_n(V) = 0.28 \exp\left(\frac{-V - 55}{40}\right).$$

Slowly Inactivating Potassium Conductance

Slowly inactivating outward currents are ubiquitous in the brain (Llinás, 1988). The currents in different structures of the nervous system have different voltage-dependent, kinetic and pharmacological properties and different names (I_D, I_{Ks}, I_{As}, I_{K2}). But they all have a low activation threshold (~ -60 mV; Storm, 1988; McCormick, 1991; Hammond and Crépel, 1992; Foehring and Surmeier, 1993), and slow, possibly multiple, inactivation rates (Storm, 1988; Spain et al., 1991b; Hammond and Crépel, 1992; Foehring and Surmeier, 1993). The main difference between the Ks conductances, besides pharmacological characteristics, is the absolute value of the time constant of inactivation and the voltage dependence of this time constant. The time constant can be from hundreds of milliseconds (Foehring and Surmeier, 1993) to several tens of seconds (Lüthi et al., 1996). Some conductances recover from inactivation much slower than they inactivate (Kv1.3 conductance; Marom and Levitan, 1994; Turrigiano et al., 1996). Hippocampal and striatal Ks conductances have both slow inactivation and slow recovery (Storm, 1988; Nisenbaum et al., 1994). In the neocortex and thalamus, deinactivation appears to be faster than inactivation (Huguenard and Prince, 1991; McCormick, 1991; Spain et al., 1991b; Hammond and Crépel, 1992; Foehring and Surmeier, 1993). These differences result in different temporal characteristics (such as long time constants produce long latencies to the first spike) and different relative strengths of memory effects. We have used a model of the neocortical Ks conductance described by Hammond and Crépel (1992) for the following reasons: (1) this conductance is well suited to a study of memory of inhibition since its slow inactivation results in a large effect on first-spike latency and its fast deinactivation allows efficient control of this effect by hyperpolarization; (2) a complete description of activation and inactivation processes is provided; (3) current-clamp recordings with pharmacological manipulations illustrate the functional role of Ks conductance.

The results presented here are probably qualitatively similar for other Ks conductances; however, the functional conclusions are likely to depend on the properties of each conductance. The activation of Ks conductances could also have important computational roles (Wang, 1993; Gutfreund et al., 1995; Hansel and Sompolinsky, 1996; Golomb and Amitai, 1997).

The slowly inactivating potassium current was described by

$$I_{Ks} = \bar{g}_{Ks} m_{Ks} h_{Ks} (V - E_K),$$

with $\bar{g}_{Ks} = 1$ mS.cm^{-2}. The activation variable obeyed first-order kinetics and its steady-state activation function was taken as (Fig. 1A)

$$m_{Ks}^{\infty}(V) = \frac{1}{1 + \exp\left(-\frac{V+44}{5}\right)}$$

(Storm, 1988; McCormick, 1991; Hammond and Crépel, 1992; Foehring and Surmeier, 1993). A voltage-independent time constant τ_{mKs} of 50 ms was used. The steady-state inactivation function was (Fig. 1A)

$$h_{Ks}^{\infty}(V) = \frac{1}{1 + \exp\left(\frac{V+74}{9.3}\right)}$$

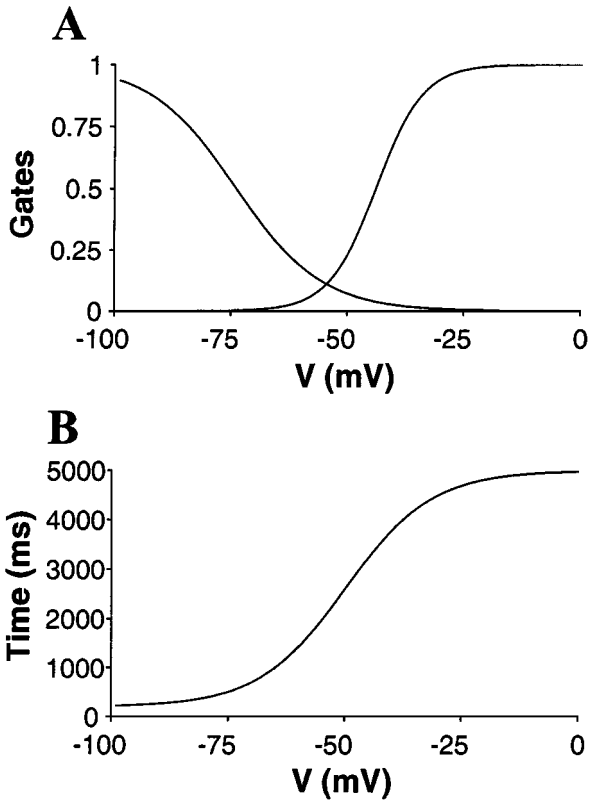

Figure 1. The slowly inactivating potassium (Ks) conductance model. **A:** Steady-state activation and inactivation functions. **B:** Inactivation time constant function.

from Hammond and Crépel (1992). The inactivation of Ks conductance at the onset of simulations was represented by $1-h_{ini}$, where h_{ini} is the initial deinactivation. The inactivation/deinactivation time constant was fitted to a sigmoid curve (Huguenard and McCormick, 1992; Wang, 1993) from the data of Hammond and Crepel (1992). It is voltage-dependent with slow inactivation at depolarized potentials and fast deinactivation at hyperpolarized potentials (Fig. 1B)

$$\tau_{hKs}(V) = 200 + \frac{4800}{1+\exp\left(-\frac{V+50}{9.3}\right)}.$$

Parameter Study

The model was defined by a number of parameters. Since we were interested in the inactivation of Ks conductance, most of the parameters were kept constant (membrane and action potential parameters, Ks activation parameters). In the initial part of the study, the Ks maximal conductance ($\bar{g}_{Ks}$) and the Ks inactivation time constant (τ_{hKs}) were varied to represent possible regulations (LeMasson et al., 1993). These two *intrinsic* parameters remained constant in the rest of the study. We defined two types of neuron: the "standard" neuron ($\bar{g}_{Ks} = 0$) and the "slowly inactivating" neuron ($\bar{g}_{Ks} = 1$). The principal *control* parameters of the model were the injected current I and the initial value of the inactivation gate h_{ini} (deinactivation level). The two control parameters are independent: (1) h_{ini} reflects the past history of the neuron (although h_{ini} is referred to as a control parameter for convenience, it actually constitutes an initial condition of the dynamical system described above); (2) I is a forcing function of the system. Note that h_{ini} can be represented by a conditioning current or a conditioning voltage (that is, a current- or a voltage-clamp protocol leading to this level of deinactivation).

In Vitro Studies

The two control parameters were varied systematically. Although h_{ini} can theoretically take any value between 0 and 1, its range is determined under physiological conditions by the kinetics of the conductance (see above). In the present case, deinactivation is faster than inactivation, so h_{ini} can be more easily increased than decreased. However, a large range of h_{ini} was explored to keep the model as general as possible. We will use the term *inactivated* (respectively, *deinactivated*) to indicate that $h_{ini} \leq h_{Ks}^{\infty}(V_{rest}) \approx 0.4$ (resp. $h_{ini} \geq h_{Ks}^{\infty}(V_{rest})$), where V_{rest} is the resting potential of the neuron.

In Vivo Studies

Cortical neurons *in vivo* discharge in a highly irregular fashion (Softky and Koch, 1993; Shadlen and Newsome, 1994). This variability arises in part because these neurons receive strongly fluctuating excitatory and inhibitory inputs (Softky and Koch, 1993; Stevens and Zador, 1998). In these conditions, the total input current that impinges on a neuron deviates largely from the perfect clamp of *in vitro* studies. Thus, properties that are observed *in vitro* are likely to be altered *in vivo*.

In a standard model of cortical discharge variability, a neuron receives a large number of afferent excitatory and inhibitory inputs representing both spontaneous

and evoked activity in cortical networks (Shadlen and Newsome, 1994). Presynaptic spike trains are in general Poisson. An important and unknown parameter of this model is the degree of synchronization in presynaptic spike trains (Softky and Koch, 1993; Stevens and Zador, 1998). The stronger the synchronization, the larger the variability of the synaptic current. A simple way to account for the degree of variability is to consider that a unitary postsynaptic potential (PSP) represents the contribution of several coincident presynaptic spikes. In this way, a set of synchronized incoming trains can be replaced by a single train with an appropriately scaled synaptic conductance.

On this basis, we defined the total synaptic current as

$$I(t) = I_{syn}(t) = g_{exc}(t)(E_{exc} - V) + g_{inh}(t)(E_{inh} - V),$$

where $E_{exc} = 0$ and $E_{inh} = -85$ mV. The total excitatory synaptic conductance $g_{exc}(t)$ was calculated as the sum of excitatory synaptic conductances elicited by presynaptic action potentials

$$g_{exc}(t) = \sigma \bar{g}_{exc} \sum_{i=1}^{n_{exc}} \alpha\left(t - t_{exc}^{i}\right) H\left(t - t_{exc}^{i}\right),$$

where $\bar{g}_{exc}$ is the maximal excitatory synaptic conductance, σ a scaling factor (see below), n_{exc} the number of presynaptic spikes, (t_{exc}^{i}) the spike arrival times generated by a Poisson process at the frequency f_{exc}, H the Heaviside function ($H(x) = 1$ if $x \geq 0$ else $H(x) = 0$), and α the function defined by

$$\alpha(t) = \frac{et}{\tau} e^{-t/\tau}$$

with $\tau = 3$ ms. The total inhibitory synaptic conductance $g_{inh}(t)$ was defined in the same way, with $\bar{g}_{inh}$ and f_{inh}.

Estimates of presynaptic frequencies have been obtained based on anatomical and electrophysiological arguments (Shadlen and Newsome, 1994). A cortical neuron receives 3,000 to 10,000 synapses, ~80% of which are excitatory (Peters, 1987). If 10% of the excitatory synapses are stimulated at 20 Hz, the range of excitatory frequencies is 4.8 to 16 kHz. If 10% of the inhibitory synapses are stimulated at 40 Hz, the range of inhibitory frequencies is 2.4 to 8 kHz. The inhibitory presynaptic frequency f_{inh} was set at 4 kHz. The excitatory frequency f_{exc} was varied to obtain a given output frequency (see below).

The synaptic conductances were derived from estimated sizes of postsynaptic potentials in neocortex. The size of EPSPs are in the range of 0.05 to 2 mV (Komatsu et al., 1988; Mason et al., 1991; Nicoll and Blakemore, 1993). The size of IPSPs are in the range of 0.1 to 1.5 mV (Deuchars and Thomson, 1995) and 0.2 to 3.5 mV (mean ~1.4 mV) at −60/−55 mV (Thomson et al., 1996). We chose 0.8 and 0.7 mV as standard sizes of EPSPs and IPSPs at resting potential, respectively. The size of IPSPs at −60 mV was 1.2 mV. The corresponding synaptic conductances were $\bar{g}_{exc} = 2.5 \cdot 10^{-3}$ and $\bar{g}_{inh} = 7 \cdot 10^{-3}$ (in mS.cm^{-2}). With these values, the range of f_{exc} was 7 to 11 kHz in order to obtain postsynaptic discharges at 10 to 70 Hz. The coefficient of variation (CV) of a 30 Hz discharge was ~0.7, well within the range of cortical variability (Softky and Koch, 1993).

Different degrees of variability were modeled for the same output frequency. The actual inhibitory presynaptic frequency and synaptic conductances were f_{inh}/σ, $\sigma \bar{g}_{exc}$, and $\sigma \bar{g}_{inh}$, where σ is in the range of 0.1 to 1. The presynaptic excitatory frequency was scaled to keep the output frequency constant. Scaling synaptic conductances or PSP sizes are the same since the two are linearly related in the range under study. Note that the lowest σ produces a CV of ~0.45 at 30 Hz, which is at the lower limit of cortical variability (Softky and Koch, 1993; Shadlen and Newsome, 1994). Unless otherwise specified, $\sigma = 1$.

Quantitative Description of Discharge Behavior

We used five numbers to describe the discharge behavior of the modeled neuron: the latency-to-first-spike, the initial frequency following the possible latency, the steady-state frequency, the time constant of frequency change, and the ratio of steady to initial frequency (ramp gain).

The following definitions were used for *in vitro* conditions. The criteria used to measure a latency in the presence of the Ks conductance were the following: (1) if the voltage remained subthreshold for 15 s, the injected current was considered to be subthreshold; (2) if the time of the first spike was >500 ms, the latency was given this duration; (3) if early spikes occurred and an interspike interval (ISI) >500 ms was found later, the latency was the total time between the beginning of the stimulation and the end of the ISI (delayed discharge); (4) otherwise the neuron discharged without delay (immediate discharge). These criteria are needed to remove

transient effects due to *Ks* activation. Though these choices are arbitrary, they have little influence on the reported results. When $\bar{g}_{Ks} = 0$, the latency was simply the time to the first spike. The initial frequency of the discharge was the frequency measured after the transitory period due to activation of Ks conductance. Calculations are outlined in Appendix B. The steady frequency was the reciprocal of the last ISI after 15 s discharge. The time constant of frequency change was obtained by a fit of the instantaneous frequency to a monoexponential function.

Closely related definitions were used for *in vivo* conditions. The latency was the mean of latencies (20 replications) obtained as described above. The coefficient of variation of the latency was defined as the standard deviation divided by the mean of latencies (20 replications). The initial frequency was the mean frequency (50 replications) measured after the transitory period due to activation of the Ks conductance at a fixed level of deinactivation. The steady frequency was the mean steady frequency (50 replications) in the last 250 ms discharge of the 15 s discharge. The time constant of frequency change was obtained by fitting the mean frequency to a monoexponential function.

Simulations

In all the simulations, a conditioning protocol was used to fixate the initial level of deinactivation h_{ini}. For the sake of simplicity, we assumed that the membrane potential always starts from the resting potential. Thus the initial conditions were $V = V_{rest}$, $x = x^{\infty}(V_{rest})$ with $x = \{m, h, n, m_{Ks}\}$, $h_{Ks} = h_{ini}$. This led to a slight underestimate in latency calculations ($\sim$20 ms for a conditioning voltage of $V_{rest} \pm 10$ mV). Numerical solutions of the differential equations were obtained using a backward Euler method, with an integration time step of 100 μs.

Results

Latency to First Spike in Vitro

The behavior of the model in response to a 4 s current step ($I = 2\ \mu\text{A.cm}^{-2}$) was studied. Figure 2 shows three typical firing patterns obtained starting from different initial levels of deinactivation (from top to bottom, $h_{ini} = 0.6, 0.4, 0.2$). In the first two cases the membrane potential gradually increased over several seconds to the action potential threshold (Figs. 2A and 2B). This rise was due to the slow inactivation of the Ks conductance which progressively allowed a stronger influence of the injected depolarizing current (Figs. 2A and 2B). The latency-to-first-spike was longer for a more deinactivated initial level (Fig. 2A) and disappeared for an initially inactivated level (Fig. 2C). In all cases the activation gate rapidly followed the voltage changes. An initial spike sometimes preceded the delay before sustained firing because of a buildup of Ks activation (Figs. 2A and 2B), much like that observed by Spain et al. (1991a) and Marom and Abbott (1994). This phenomenon would not be observed with faster activation kinetics (such as $\tau_{mKs} = 10$ ms).

Latency-to-first-spike was systematically studied by varying the amplitude of the input current ($0 \leq I \leq 5\ \mu\text{A.cm}^{-2}$), the initial level of deinactivation ($0 \leq h_{ini} \leq 1$), the time constant of Ks (using a voltage-independent time constant τ_{hKs} between 1 and 5 s), and the maximal conductance of Ks ($0 \leq \bar{g}_{Ks} \leq 2$ mS.cm^{-2}). The latency decreased with increasing amplitude of the input current for different h_{ini} (Fig. 3A). The latencies were long and occurred over a large range of injected currents when the Ks conductance was initially strongly deinactivated. The latencies were smaller and appeared only for a narrow range of currents for initial inactivated states. Each curve was delimited by a minimal current (subthreshold) and a maximal current (immediate discharge). As a control, no delays longer than $\sim$250 ms were obtained (using the same discretization step as for the model with Ks conductance) when a Ks conductance was absent (Fig. 3A, inset). The delay increased with h_{ini} (Fig. 3B), τ_{hKs} (Fig. 3C), and $\bar{g}_{Ks}$ (Fig. 3D).

An analytical description of the role of Ks inactivation in the discharge behavior of the neuron was developed (Appendix A). Equation (4) provides a good qualitative explanation of the simulation results. Latency-to-first-spike varies linearly with $-\ln(I - \alpha_I)$, $\ln(h_{ini} - \alpha_h)$, τ_{hKs}, $-\ln(1/\bar{g}_{Ks} - \alpha_g)$, where α_I, α_h, and α_g are parameters. These equations were appropriate to fit the data in Fig. 3. Comparison of Eqs. (4) and (6) in Appendix A helps explaining the role of the Ks conductance. First, the inactivation time constant of Ks substitutes for the membrane time constant. Second, the dependence on the injected current is $-\ln(1 - \alpha_I/I)$ in the Lapicque model and becomes $-\ln(I - \alpha_I)$ in the Ks neuron. Both relations have the same asymptotic behavior as $I \to \alpha_I^+$ but differ for large values of I. The former stops changing rapidly

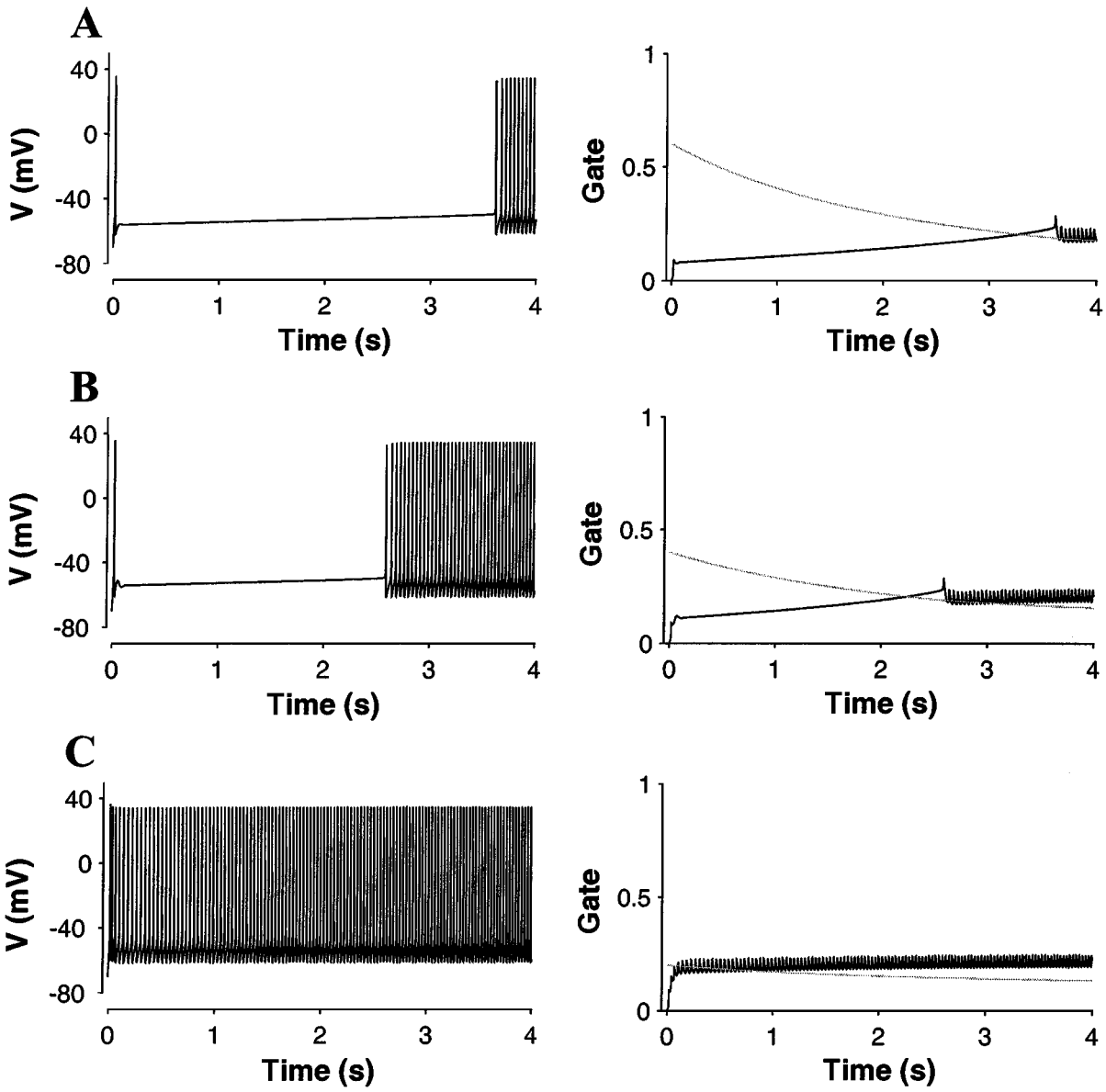

Figure 2. Latency-to-first-spike. Left-hand column shows voltage variations. Right-hand column shows Ks activation (plain line) and inactivation (gray line) gates. Injected current was $I = 2\ \mu\text{A.cm}^{-2}$. Initial deinactivation was 0.6 (A), 0.4 (B), 0.2 (C).

since it reaches an asymptote at 0. The latter decays more progressively.

Discharge Behavior in Vitro

The pattern of discharge was influenced by both I and h_{ini} (Fig. 4A). Three typical patterns were found: a delay followed by an increase in frequency (Fig. 4A1), an immediate discharge at increasing frequency (Fig. 4A2), and a discharge at approximately constant frequency (Fig. 4A3). There was also a weakly adaptating discharge pattern for low h_{ini} (not shown). The instantaneous frequency (inverse of ISIs) of the discharge was calculated for different I (Fig. 4B) and h_{ini} (Fig. 4C). At large I, discharge began immediately. Smaller currents resulted in nonzero latency-to-first-spike (Fig. 4B). In both cases a brief transitory period

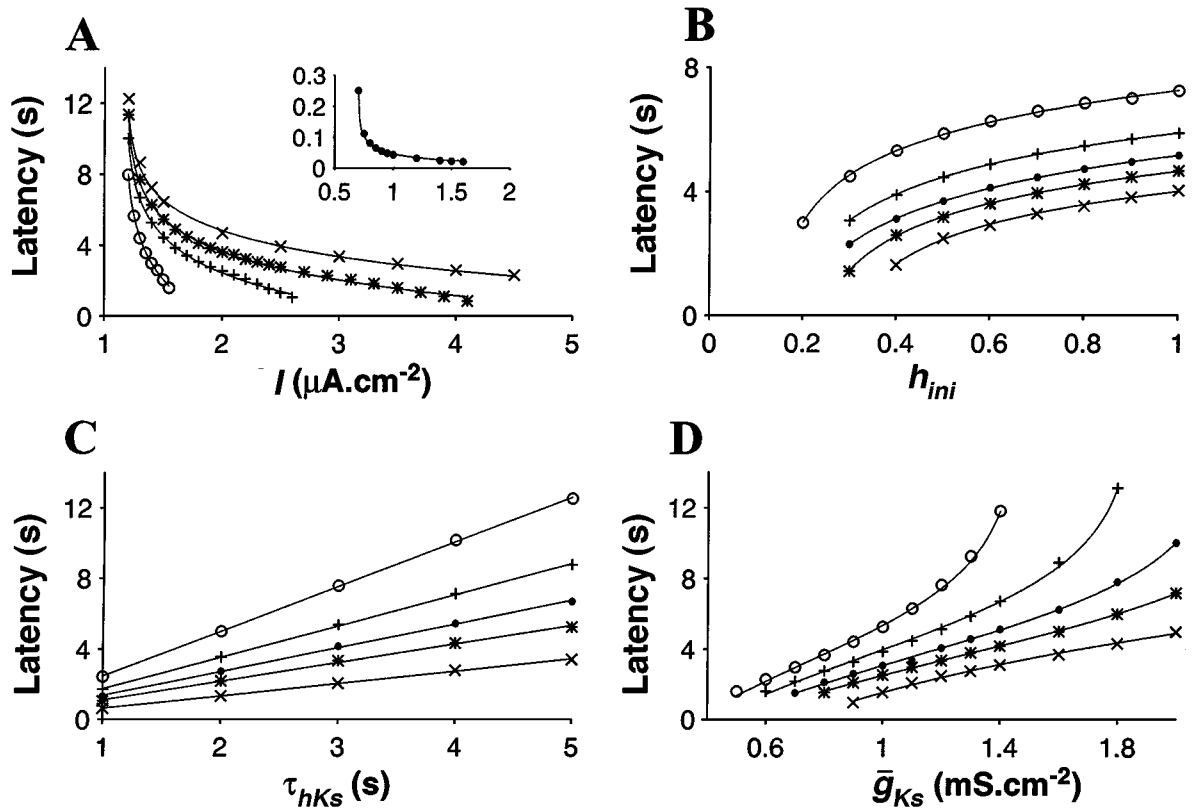

Figure 3. Parameter study of latency-to-first-spike. Parameters that are not specified are as indicated in Methods. Fits were obtained from equation (4) in Appendix A. **A:** Latency versus injected current for different h_{ini} (cross: 1; star: 0.6; plus: 0.4; open dot: 0.2). Unbroken lines are best fits to $y = \alpha \ln(x + \beta) + \gamma$. Inset is the case with $\bar{g}_{Ks} = 0$ (best fit to $y = \alpha \ln(\beta - 1/x)$). **B:** Latency versus h_{ini} for different injected currents (cross: 2.4; star: 2; closed dot: 1.8; plus: 1.6; open dot: 1.4, in μA.cm^{-2}). Plain lines are best fits to $y = \alpha \ln(x + \beta) + \gamma$. **C:** Latency versus time constant for different injected currents. Same symbols as in **B**. Unbroken lines are best linear fits. **D:** Latency versus maximal conductance for different injected currents. Same symbols as in **B**. Unbroken lines are best fits to $y = \alpha \ln(1/x + \beta) + \gamma$.

due to Ks activation buildup was followed by a mono-exponentially increasing discharge (time constant of ~2.6 s). Initial and steady frequencies (see definitions in Methods, Appendix B, and below) increased with the injected current (Fig. 4B). The influence of h_{ini} is shown in Fig. 4C. All the discharges terminated at the same steady frequency for a given I. For immediate discharges, the initial frequency decreased as h_{ini} increased. For delayed discharges, the initial frequency varied little with h_{ini}. The frequency decreased to steady state for low h_{ini} (0.1).

We have developed a method to explain the whole discharge behavior and to rigorously define the initial discharge frequency. Since Ks inactivation is very slow, the discharge frequency at any given time is close to the steady frequency obtained using the inactivation gate as a parameter equal to the deinactivation level at this time. We calculated the steady frequency of the discharge as a function of the deinactivation level considered as a constant parameter (h_{param})—that is, the time constant of Ks conductance was taken to be infinite (Fig. 5A). We found that the frequency decreased in a quasi-linear fashion for each current and then abruptly waned to zero as h_{param} increased (Fig. 5A). This suggests that repetitive firing (for parameter h_{param}) begins at a nonzero frequency (see Appendix B). We defined the initial frequency of the discharge as this numerically estimated onset frequency (crosses in Fig. 5A). The way to read the plot in Fig. 5A is the following (Fig. 5A, inset). Choose a h_{param} (e.g. 0.6) and an injected current (such as $I = 3$). The frequency remains at 0 until the inactivation gate reaches ~0.4. At this level, the frequency jumps at ~15 Hz (cross) and then follows the curve until the steady state (star). We calculated

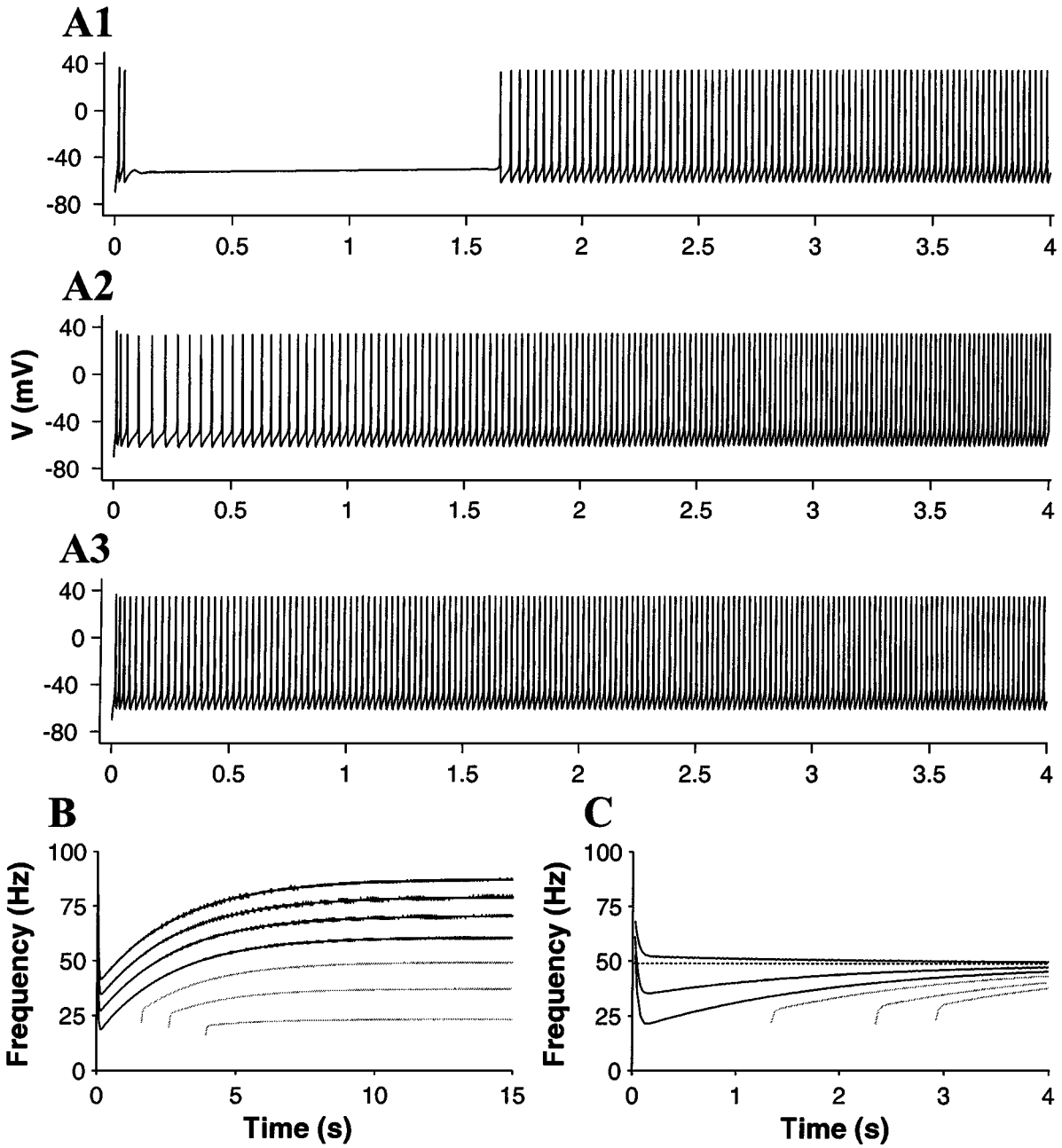

Figure 4. **A:** Influence of I and h_{ini} on discharge frequency (A1: $I = 2.4$, $h_{ini} = 0.4$; A2: $I = 2.8$, $h_{ini} = 0.4$; A3: $I = 2.4$, $h_{ini} = 0.2$). **B:** Instantaneous firing rate during a 15 s discharge. Initial deinactivation level was 0.4. From top to bottom, the injected current was 4, 3.6, 3.2, 2.8, 2.4, 2, and 1.6 (μA.cm^{-2}). Gray lines indicate delayed discharges. In this case, early spikes and the first spike after the delay were not taken into account in the calculus of frequency. **C:** Instantaneous firing rate during a 4 s discharge. The injected current was 2.4 μA.cm^{-2}. From top to bottom, h_{ini} was 0.1, 0.2, 0.3, 0.4, 0.6, and 0.8. The steady frequency after 15 s discharge is indicated by a dashed line.

the discharge frequency as a function of I. The initial and steady frequencies were a threshold close-to-linear function of I for different h_{ini} (Fig. 5B). The ramp gain (see Methods) increased with I and h_{ini} for delayed discharges (Figs. 5C and 5D). It decreased with I (since initial and steady frequencies increased with I in a similar way; Fig. 5B) and remained constant with h_{ini} for immediate discharges (Figs. 5C and 5D). These results

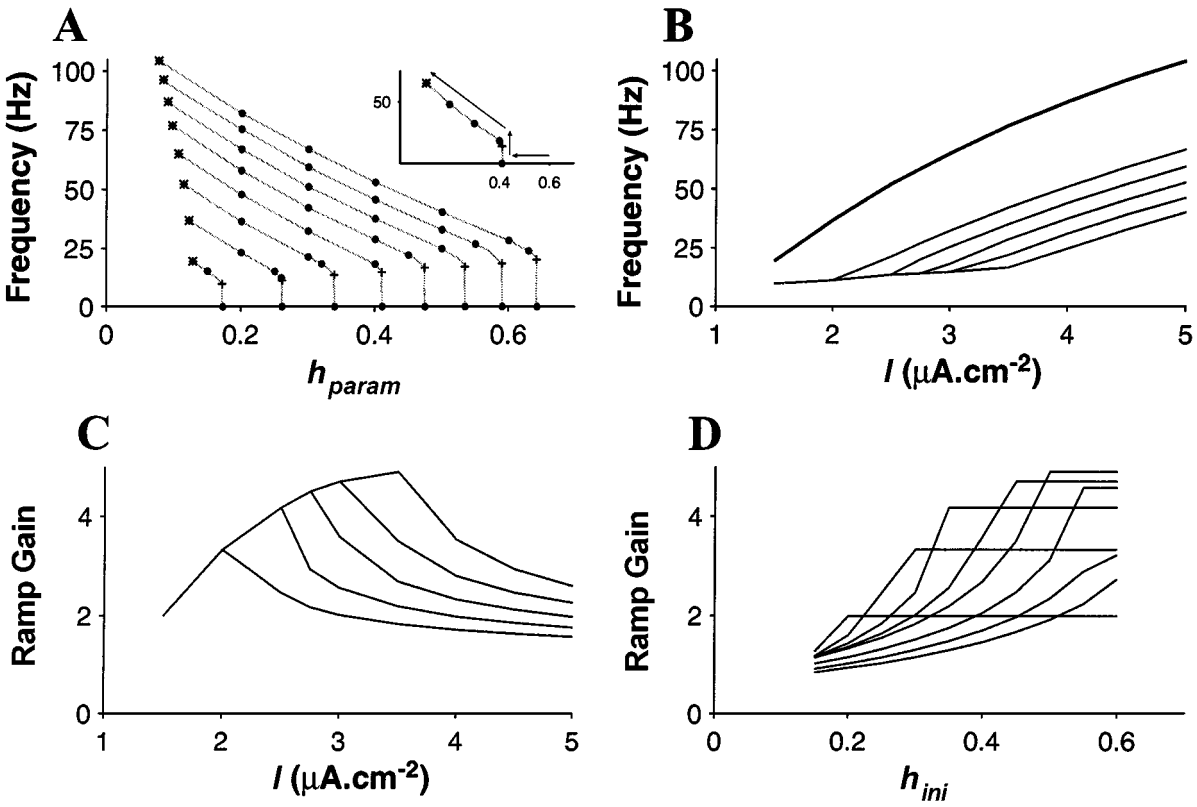

Figure 5. **A:** Frequency versus h_{param} for infinitely slow inactivation with different injected currents (from top to bottom: 5, 4.5, 4, 3.5, 3, 2.5, 2, 1.5 μA.cm^{-2}). Symbols are calculated points. The onset frequency of firing is indicated by a plus symbol. The steady frequency calculated with normal inactivation is indicated by a star symbol. **B:** Initial (normal lines) and steady (thick line) frequency versus injected current for different h_{ini} (from top to bottom: 0.3, 0.35, 0.4, 0.45, 0.5). **C:** Ramp gain (steady frequency/initial frequency) versus injected current for different h_{ini} (from top to bottom: 0.5, 0.45, 0.4, 0.35, 0.3). **D:** Ramp gain versus h_{ini} for different injected currents (from left to right: 1.5, 2, 2.5, 3, 3.5, 4, 4.5, 5 μA.cm^{-2}).

show that a wide variety of ramp firing patterns can be built by altering the control parameters.

The discharge pattern is determined by the control parameters I and h_{ini}. However, h_{ini} is not a directly accessible physiological parameter, since it results from prior conditioning of the neuron—that is, a current clamp (I_{cond}) of a given duration and intensity that leads to this level of deinactivation. To understand how a neuron should be stimulated to obtain a given pattern of discharge we determined the relation between h_{ini} and I_{cond}. We used the kinetic model of Ks inactivation to calculate the deinactivation reached after a conditioning period ($0 \leq t \leq 3$ s) at subthreshold conditioning potentials (Fig. 6A and inset). The starting deinactivation level was the steady-state deinactivation level at -50 mV (that is, the maximal subthreshold depolarization during interspike intervals). It corresponds to the least favorable case in which conditioning starts while the neuron is discharging. Figure 6A helps to evaluate the physiological relevance of conditioning. It shows that substantial deinactivation occurs for 250 to 500 ms of hyperpolarization at -80 mV (see Discussion). We then derived h_{ini} as a function of the conditioning voltage. The conditioning voltage was translated into a conditioning current (I_{cond}) using the I/V curve of the neuron. The relation between h_{ini} and I_{cond} is reconstructed in Fig. 6B for different times of conditioning. This relation was close to linear. Thus the previous considerations on a control of frequency by I and h_{ini} can be extended to I and h_{ini}.

Discharge Behavior in Vivo

The question arises whether Ks conductance can also produce delay-to-firing under conditions of random

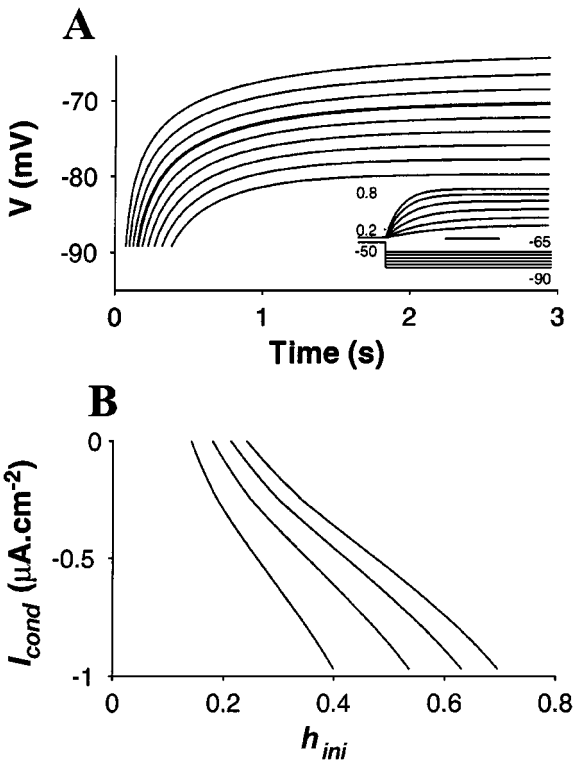

Figure 6. **A:** Deinactivation of Ks conductance as a function of time and conditioning potential. Each curve corresponds to a h_{ini} (from top to bottom 0.25, 0.3, 0.35, 0.4 (strong line), 0.45, 0.5, 0.55, 0.6, 0.65) and indicates the time it takes to increase the Ks inactivation gate from $h_{Ks}^{\infty}(-50) = 0.07$ to h_{ini} at a given conditioning potential. Inset is the conditioning protocol (top: $h(t)$; bottom: voltage). Calibration bar is 1 s. **B:** Conditioning current versus h_{ini} for different conditioning durations (from left to right, 150, 250, 350, and 450 ms).

synaptic drive (see Methods). The discharge of a slowly inactivating neuron (Fig. 7A) at two different h_{ini} is shown in Fig. 7B. The steady-state frequency was ~15 Hz. The response was characterized by large fluctuations in membrane potential. Delayed discharge was observed only for fully deinactivated initial states (Fig. 7B). These observations differ from the results obtained *in vitro*.

Mean latency-to-first-spike was calculated for different f_{exc} and h_{ini} at different degrees of variability (σ). We first considered the case where $\sigma = 1$. This latency was plotted against the steady-state discharge frequency (Fig. 7C). For the sake of comparison, the *in vivo* and *in vitro* data (taken from Fig. 3A) are shown in the same plot (Fig. 7C). Mean latencies were shorter by an order of magnitude for *in vivo* than *in vitro*. The longest latencies were found at low stimulation frequency and in fully deinactivated states (Fig. 7C). The latency was calculated for different σ and then plotted against the size of the unitary EPSPs (Fig. 7D). As expected, the longest latencies occurred with small EPSPs (low σ) but were still considerably shorter than *in vitro*. In addition to being short, the calculated latencies were also highly variable. The CV of the latency was above 0.5 for any $\sigma > 0.5$ (Fig. 7D, inset).

These results indicate that the presence of Ks conductance has an actual influence on latency-to-first-spike *in vivo*. However, this influence depends dramatically on the variability of synaptic inputs. At a realistic degree of variability, latency was mainly determined by random crossings of the spike threshold due to rapid stochastic variations in membrane potential. Thus the Ks inactivation process is probably not suitable for producing a reliable latency-to-first-spike at the single neuron level *in vivo*.

The main action of the Ks conductance was on the mean discharge frequency of the neuron. An example of instantaneous frequency is shown in Fig. 7E. Figure 7F shows the mean firing rate of a 15 s discharge for different h_{ini}. The mean frequency increased exponentially with a time constant $\tau_f \approx 2.6$ s (that is, $\sim \tau_{hKs}(-50)$). This change paralleled the slow inactivation of the Ks conductance at the depolarized potentials encountered during synaptic stimulation (Fig. 7F, inset).

Figure 8 depicts the quantitative analysis of firing frequency for *in vivo* conditions (compare to Fig. 5). Several trends were common to *in vivo* and *in vitro* conditions. The discharge frequency decreased with h_{param} (Fig. 8A). The initial and steady frequencies increased with the stimulation frequency f_{exc} (Fig. 8B). The ramp gain decreased with f_{exc} for large h_{ini} (Fig. 8C) and increased with h_{ini} (Figs. 8D). However, there were also some specific *in vivo* features. There was no sharp transition to zero-frequency discharge as h_{param} increased (Fig. 8A). Thus, the behaviors were similar at low and high frequencies (Fig. 8B), with a linear change in ramp gain with f_{exc} (Fig. 8C). The ramp gain was also weakly dependent on the stimulation frequency (and thus on the discharge frequency) over a wide range of h_{ini} and increased with h_{ini} (Figs. 8C and 8D). This trend was also observed *in vitro*, but only at higher frequencies (>100 Hz) (Figs. 5C and 5D). These relations held more strictly at low h_{ini} (Fig. 8D). Since the steady inactivation level during synaptic stimulation at 8 to 12 kHz is 0.05 to 0.1, deinactivation from this value sets the

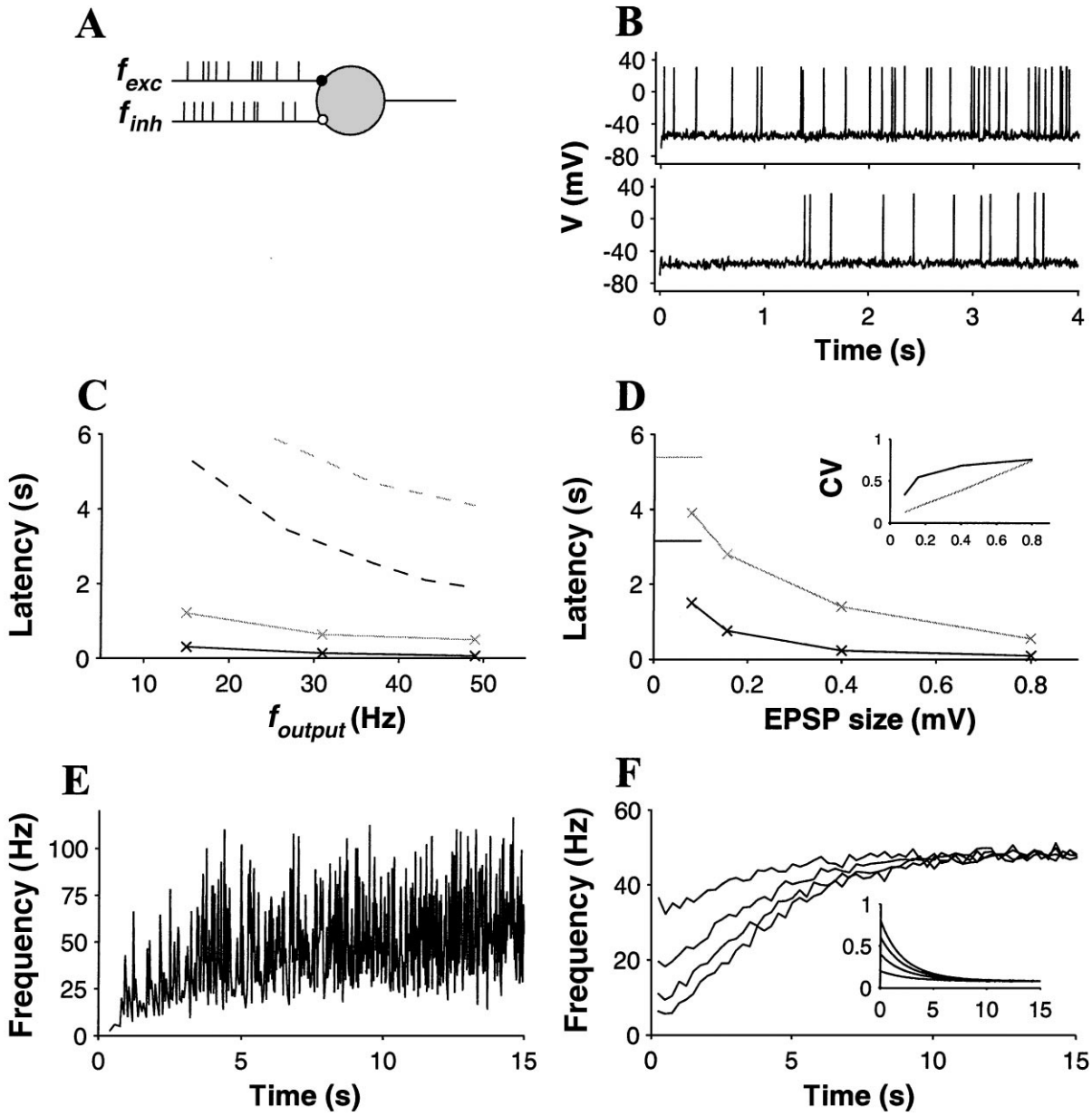

Figure 7. Response of a single neuron *in vivo*. **A:** The neuron receives two presynaptic spike trains (closed circle: excitatory synapse; open circle: inhibitory synapse). **B:** Discharge of the neuron model for $f_{exc} = 8$ kHz, $f_{inh} = 4$ kHz, $h_{ini} = 0.4$ (top), and $h_{ini} = 1$ (bottom). The same input was used in the two simulations. **C:** Latency versus steady-state output frequency for $h_{ini} = 0.4$ (plain line) and $h_{ini} = 1$ (gray line). Variability $\sigma = 1$. Stimulation frequency was $f_{exc} = 8$, 9, 10 kHz (from left to right), and $f_{inh} = 4$ kHz. Output frequency was calculated as the mean over 20 replications of 4 s discharge at steady-state inactivation. The *in vitro* data from Fig. 3A are replotted using the steady-state I/f curve of Fig. 5B: $h_{ini} = 0.4$ (dashed line), $h_{ini} = 1$ (gray dashed line). **D:** Latency versus EPSP size for $h_{ini} = 0.4$ (plain line) and $h_{ini} = 1$ (gray line). Plain and gray lines on left border indicate the latency *in vitro*. Stimulation frequency was $f_{exc} = 9$ kHz and $f_{inh} = 4$ kHz. Inset is the CV of latency plotted against EPSP size. **E:** Instantaneous discharge frequency for $h_{ini} = 0.6$, $f_{exc} = 10$ kHz, $f_{inh} = 4$ kHz. **F:** Mean discharge frequency (50 replications) for $f_{exc} = 10$ kHz and $f_{inh} = 4$ kHz and for different h_{ini} (from top to bottom: 0.2, 0.4, 0.6, 0.8). Inset is the time course of inactivation during the discharge. Bin for mean frequency calculation is 250 ms.

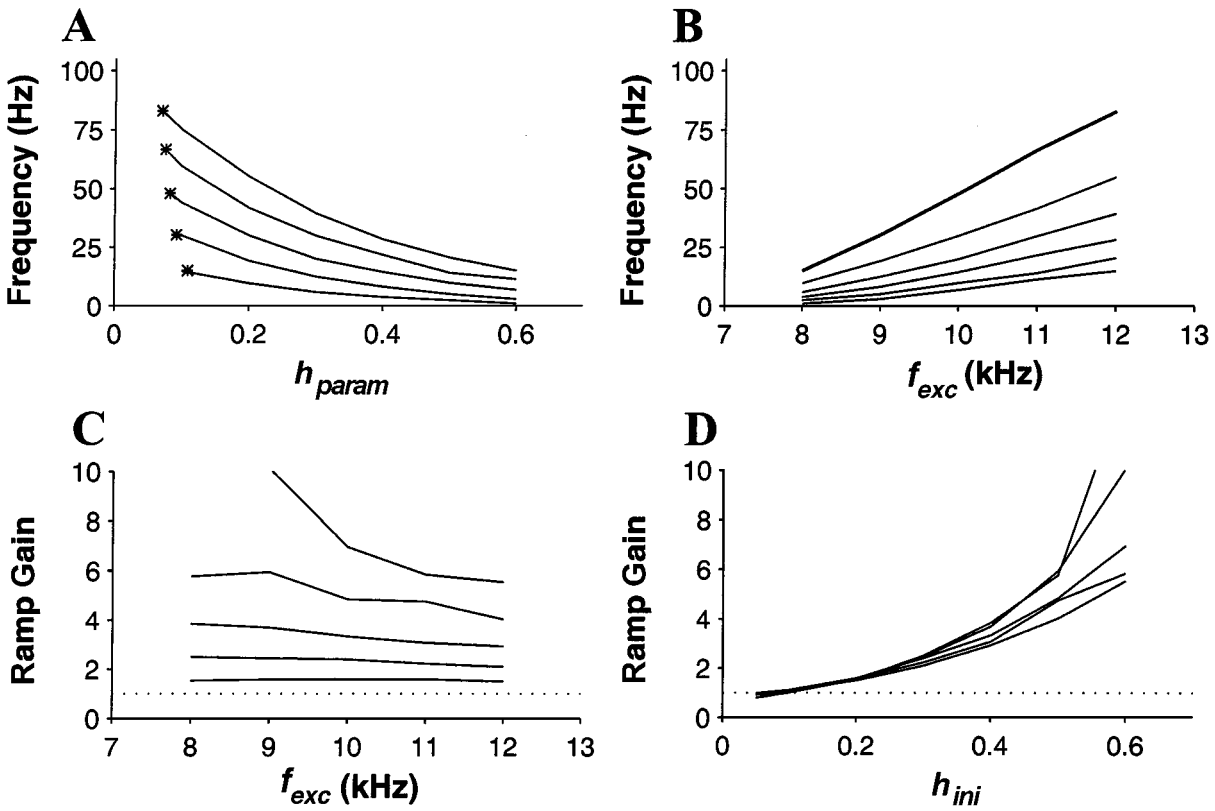

Figure 8. **A:** Mean discharge frequency (over 4 s) versus h_{param} in the case of infinitely slow inactivation for different excitatory stimulation frequencies (from bottom to top: $f_{exc} = 8, 9, 10, 11, 12$ kHz; $f_{inh} = 4$ kHz). The steady frequency is indicated by a star. **B:** Mean initial (normal lines) and steady (thick line) frequency versus excitatory frequency for different h_{ini} (from top to bottom, 0.2, 0.3, 0.4, 0.5, 0.6). **C:** Ramp gain (steady frequency/initial frequency) versus f_{exc} for different h_{ini} (from top to bottom: 0.6, 0.5, 0.4, 0.3, 0.2). Dashed line is a unit gain. **D:** Ramp gain versus h_{ini} for different f_{exc} (from top to bottom: 8, 9, 10, 11, 12 kHz).

ramp gain of the discharge independent of the injected current. Thus, each control parameter has a specific, independent influence in these conditions: f_{exc} sets the steady frequency and h_{ini} the gain.

We showed that the mean discharge of the modeled neuron *in vivo* displays a ramp pattern. This suggests that it can convey information on the time of the first spikes. We thus asked whether a population of ramp-firing neurons could provide instantaneous information on spike latency. Any threshold device could be used to decode this information. We chose a standard "postsynaptic" neuron ($\bar{g}_{Ks} = 0$) as a decoding device in order to evaluate how a target neuron outside the neocortex (e.g. a motoneuron) could convert cortical signals into behavioral outputs.

The discharge behavior of the postsynaptic neuron receiving inputs from a population of presynaptic slowly inactivating neurons (similar to the single neuron *in vivo*) was tested (Fig. 9A). The postsynaptic neuron received only excitatory signals. The size of the presynaptic population ($N = 40$) was chosen to obtain substantial latency effects in the midrange of presynaptic stimulation frequencies ($f_{exc} = 8$ to 10 kHz. In these conditions, the presynaptic neurons discharged in the range of 15 to 50 Hz and the discharge of the postsynaptic neuron (f_{post}) was in the range of 10 to 60 Hz. The relationship between f_{post} and f_{exc} was approximately linear. In the following text, we used f_{post} as an index of presynaptic stimulation since it was more meaningful than f_{exc}.

The postsynaptic neuron discharged with a progressively longer latency as h_{ini} increased (Fig. 9B). The instantaneous firing frequency of this neuron increased exponentially with the time constant τ_f (Fig. 9B, inset). The mean latency-to-first-spike decreased with f_{post} (that is, the stimulation frequency) (Fig. 9C) and

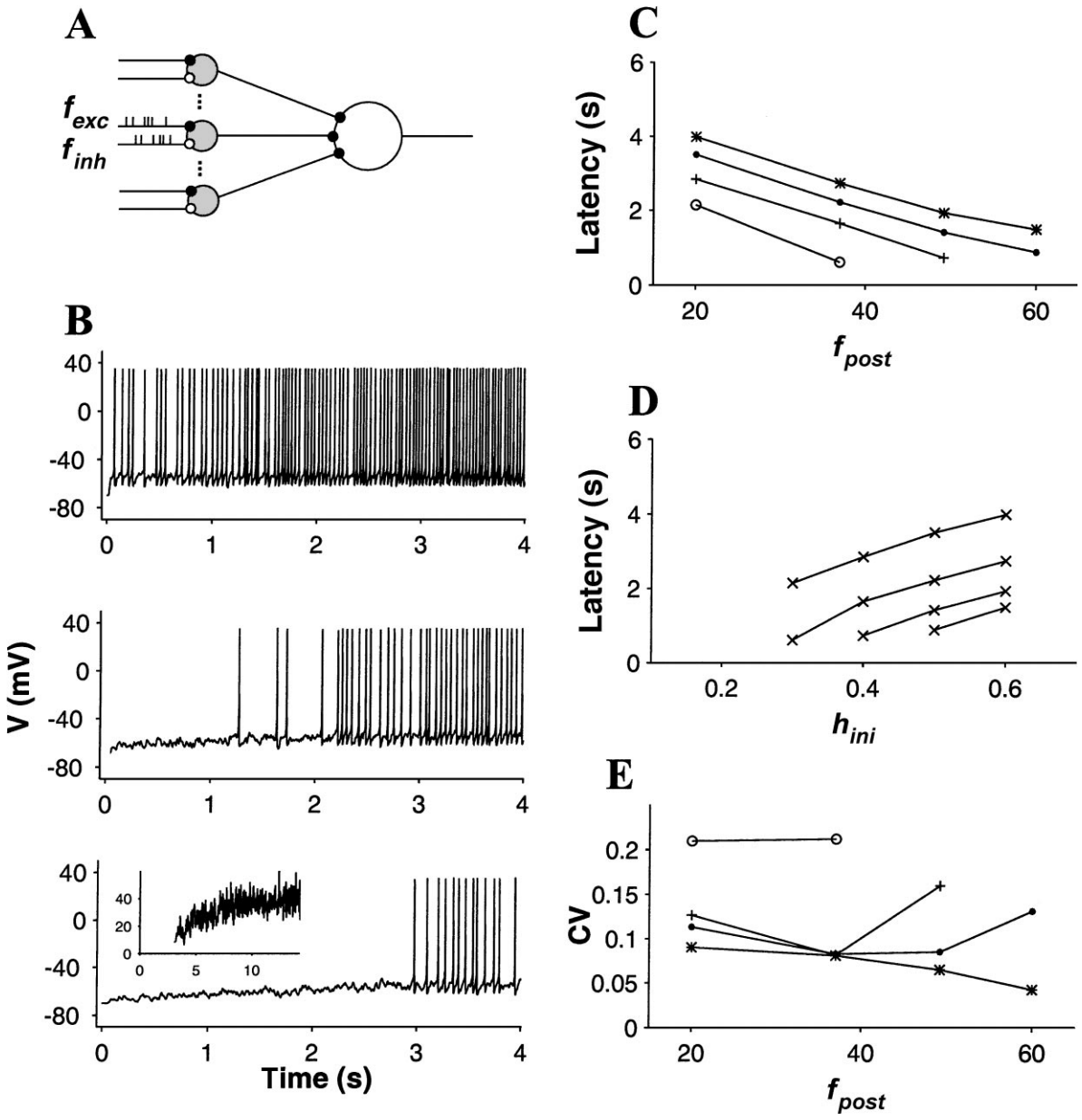

Figure 9. **A:** The convergent network. Same symbols as in Fig. 7A. **B:** Discharge of the postsynaptic neuron in response to 40 presynaptic inputs for different h_{ini} (from top to bottom, 0.2, 0.4, 0.6; $f_{exc} = 9$ kHz; $f_{inh} = 4$ kHz). Inset is the instantaneous frequency (Hz) of the corresponding discharge over 15 s. **C:** Mean latency (20 replications) versus f_{post} for different h_{ini} (star: 0.6; closed dot: 0.5; plus: 0.4; open dot: 0.3). **D:** Mean latency (20 replications) versus h_{ini} for different f_{post} (from top to bottom, 20, 37, 49, 60 Hz—that is, $f_{exc} = 8.5$, 9, 9.5, 10 kHz). **E:** Coefficient of variation of the latency versus f_{post} for different h_{ini} (same symbols as in C).

increased with h_{ini} (Fig. 9D). These trends were similar to those found *in vitro* (Figs. 9C and 3A, Figs. 9D and 3B). Since there is a stochastic component in the behavior of the network, the latencies can vary from trial to trial. However, the variability of the latency (CV) was dramatically lower than for a single neuron (Fig. 9E).

These results demonstrate that the postsynaptic neuron preserves an ordered relationship between the latency and h_{ini} and the stimulation frequency. Thus,

although the presynaptic neurons discharged without delay and had a highly variable instantaneous frequency (see above), the decoding neuron was able to suppress noise and to recover the two discharge properties due to Ks conductance: latency-to-first-spike and exponentially increasing instantaneous frequency following the delay. Generally, the results obtained for a population depend on the model of the synaptic inputs in the same way as the results obtained for a single neuron (see above). Thus, Ks inactivation is suitable for producing reliable latency within neuronal populations, although our results provide only a rough estimate of the size of the appropriate populations.

The presence of synaptic interactions within a population should influence the time course of frequency changes. We explored this using the same set of 40 neurons assembled in a fully connected excitatory network (recurrent network; Fig. 10A). Interneuronal synaptic currents had an instantaneous rise and an exponential decay (3 ms time constant). Synaptic conductance was $\bar{g}_{syn} = 0.1$ mS.cm^{-2} leading to EPSP of 0.5 mV at resting potential. All the neurons had the same initial deinactivation level and received individually randomized stochastic excitatory inputs at frequency f_{exc}. The same set of inputs was used for each simulation. We compared the influence of the "feedforward" stimulation (excitatory input at frequency f_{exc}) and the "lateral" stimulation due to the recurrent connections. For this we contrasted the pattern of frequency increase during pure feedforward processing (Fig. 10B) and feedforward + lateral processing for the same steady state (Fig. 10C). In the latter case the frequency increase departed from the exponential trend with time constant τ_f due to Ks inactivation and became linear for 1-2τ_f. Lateral interactions also allowed frequency increases at variable rates as f_{exc} increased (Fig. 10C). This was not seen *in vitro* (see Fig. 4B), or with pure feedforward processing (Fig. 10B). The analytical model in Appendix C (Eq. (7)) illustrates the qualitative difference between the dynamics of frequency increase in the recurrent and nonrecurrent networks (Fig. 10D). Furthermore, in the presence of lateral interactions a smaller amount of injected current is required to obtain the same steady-state frequency. Thus, the initial frequencies are smaller and vary in a smaller range in the recurrent case than in the nonrecurrent case for the same steady-state frequencies (Fig. 10D). We calculated the slope of frequency increase in the first 4 seconds of the discharge as a function of f_{exc} and $\bar{g}_{syn}$. The slope increased linearly with the stimulation frequency (Fig. 10E) and nonlinearly with the synaptic conductance (Fig. 10F). These results are well accounted for by an analytical steady-state frequency approximation of the network (Appendix C).

Discussion

There are three main findings. First, a slowly inactivating potassium conductance can shape the discharge behavior of a neuron *in vitro* according to simple laws that specify the latency-to-first-spike and the pattern of frequency change (ramp firing) as a function of the biophysical characteristics of the neuron, the current state of the neuron (initial deinactivation) and the injected current. Second, control of first spike latency is lost at the single-cell level under random synaptic stimulation but recovers at the population level. Third, frequency changes at variable rate are made possible by the combined action of Ks inactivation and synaptic interactions in a network.

Effects of Ks Inactivation Under Current Clamp

It has been proposed that Ks conductances influence the latency-to-first-spike and the pattern of discharge in many neurons (Byrne et al., 1979; Byrne, 1980; Getting, 1983; Storm, 1988; Bargas et al., 1989; Huguenard and Prince, 1991; Spain et al., 1991; Hammond and Crepel, 1992; Marom and Abbott, 1994; Nisenbaum et al., 1994; Wang and McKinnon, 1995; Turrigiano et al., 1996; Gabel and Nisenbaum, 1998). The present study describes electrophysiological properties that result from the presence of Ks conductance in a biophysical model of a neuron. The model reproduces most of the properties observed experimentally and provides new information on the role of Ks conductance based on a systematic exploration of parameters.

Latency-to-first-spike due to inactivation of the Ks conductance was reproduced under current clamp in this model and analyzed as a function of the parameters of the model. Simulations first showed that the latency is a decreasing logarithmic function of the injected current, consistent with the results of Getting (1983), Lanthorn et al. (1984) and McCormick (1991). At low initial deinactivation levels, there was delay-to-firing only over a narrow range of injected currents and the slope of the relationship is steep (a small change in current causes a large change in latency). Increasing

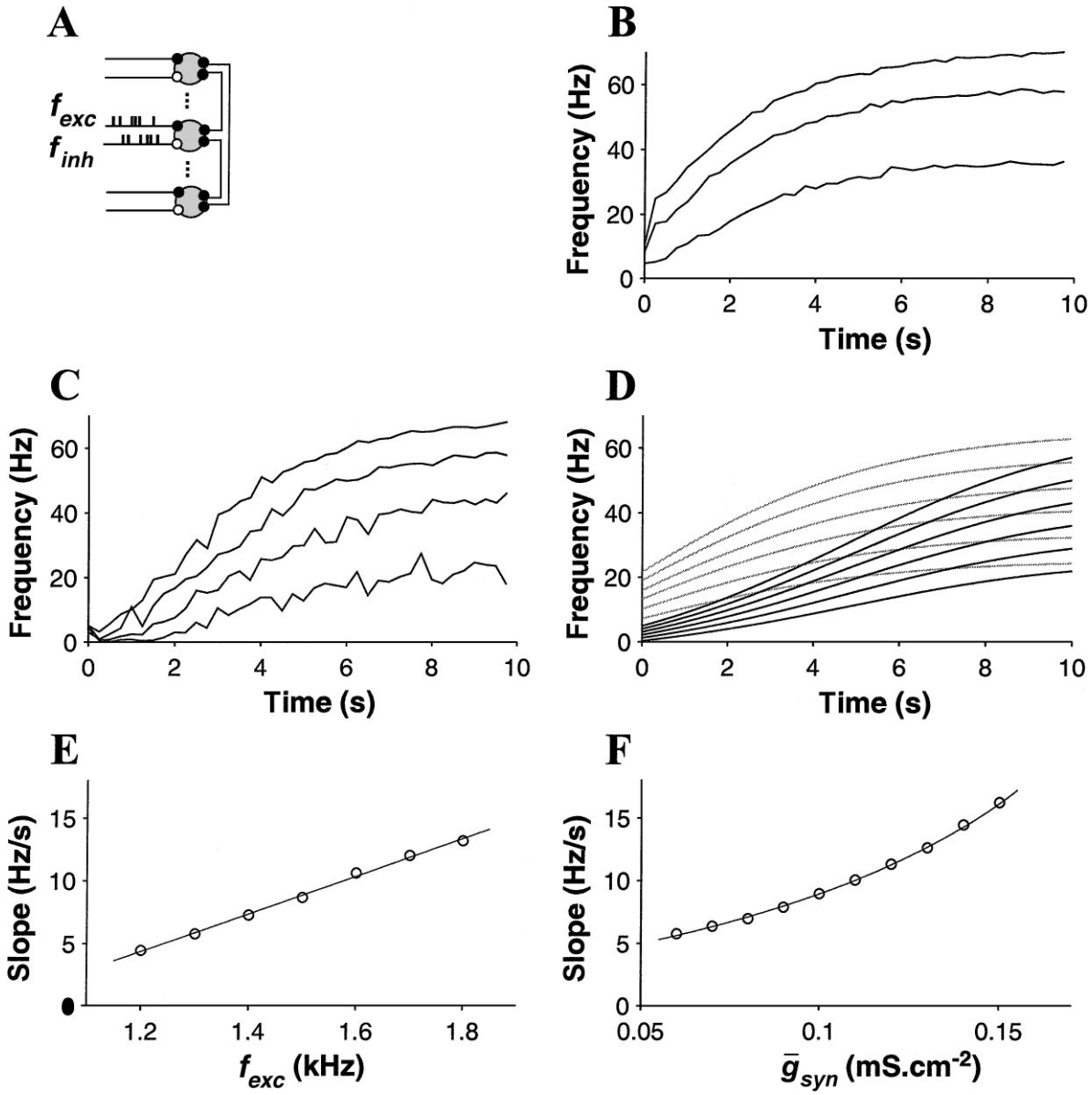

Figure 10. **A:** The recurrent network. Same symbols as in Fig. 7A. **B:** Mean network discharge frequency for $h_{ini} = 0.4$ and null synaptic interactions (from bottom to top, $f_{exc} = 2, 2.9, 3.7$ kHz). **C:** Mean network discharge frequency for $h_{ini} = 0.4$ and normal synaptic interactions (from top to bottom $f_{exc} = 1.1, 1.3, 1.5, 1.7$ kHz). Bin for mean frequency calculation is 250 ms. **D:** Mean network discharge frequency obtained from Eq. (7) in Appendix C. Recurrent (normal lines; $g = 0.05$; from bottom to top, $I = 7.2, 7.32, 7.44, 7.56, 7.68, 7.8$) and nonrecurrent (gray lines; $g = 0$; I was adjusted to obtain the same steady-state frequencies) cases are shown. **E:** Slope of frequency increase versus f_{exc}. The slope was obtained as the best linear fit of the first 4 seconds of discharge. Unbroken line is best linear fit (Eq. (9) in Appendix C). **F:** Slope of frequency increase versus $\bar{g}_{syn}$. Same definition as in **E**. Unbroken line is best fit to $y = (\alpha + \beta x)/(1 + \gamma x)$ (Eq. (9) in Appendix C).

h_{ini} decreases this slope and enlarges the domain of inputs corresponding to a given range of latencies. Thus a broader range of inputs can be represented by the same range of latencies. Latency-to-first-spike is determined by the time to reach the threshold for discharge. Accordingly the threshold has a definite influence on latency. Our model neuron has a threshold ~ -50 mV that is within the range of thresholds for a wide

variety of neurons. Irrespective of the threshold, the magnitude of the latency effects depends on the presence of Ks conductance (milliseconds versus seconds; see Fig. 3A). The latency also increases logarithmically with h_{ini}, in agreement with the observation of Getting (1983) of an apparent logarithmic dependence between latency-to-first-spike and prepulse hyperpolarization. The variations in latency with Ks maximal conductance must be considered cautiously, since a long-lasting large potassium current could reduce the driving force for K^+ ions, which would itself decrease the current. This mechanism is not included in the model, which could explain the discrepancy with the results of Turrigiano et al. (1996), who reported an apparently bounded variation of the delay to first spike with $\bar{g}_{Ks}$.

The whole model was reduced so that Ks inactivation represented the only dynamical variable to provide a theoretical description of the effects of Ks inactivation. Analytical solutions for membrane potential (before discharge), Ks inactivation and latency-to-first-spike were obtained in terms of the biophysical parameters of the model. The reduced model gives results qualitatively similar to those obtained by simulation of the whole model. The analytical formulae reveal that the Ks conductance replaces the leak conductance to determine the time of the first spike, with two significant effects. First, proportionality to membrane time constant is replaced by proportionality to the Ks time constant, which explains the long delays-to-firing. Second, the Ks conductance improves the mapping between injected currents and latencies (see above).

A fraction of Ks current during a ramp is a window current since the steady-state inactivation at potentials encountered during the ramp (approximated by h_θ in Appendix A) is substantial in our model. The latency depends directly on h_θ (see Eq. (4)). Therefore latency-to-first-spike depends not only on the rate of inactivation of Ks conductance but also on a "noninactivating" component. We estimated the contribution of this component for wide ranges of I and h_{ini} to be up to 30% of the latency—that is, the latency was reduced by 30% when $h_\theta = 0$.

Nisenbaum et al. (1994) observed in medium spiny neurons of the striatum that the slope of the ramp before the first spike increased with the mean level of depolarization encountered during the ramp but was independent of the initial level of inactivation. The same properties were found in our model. It was also found in different neurons that the slope of the ramp associated with Ks increases throughout the delay (Nisenbaum et al., 1994; Turrigiano et al., 1996). This was not the case in our model as the slope remained constant until the very end of the ramp. This difference could be due to the activation of other subthreshold conductances during the ramp (such as persistent sodium conductance; see Nisenbaum et al. 1994). It could also arise from the model of the Ks conductance. For example, the Kv1.3 slowly inactivating potassium current model (Marom and Levitan, 1994), which has a state-dependent rather than a voltage-dependent inactivation process, produces ramps with increasing slope during the delay (as evidence by unpublished simulations).

After a possible delay, current injection results in repetitive firing. The instantaneous frequency of the discharge is proportional to the instantaneous Ks inactivation level after a brief transitory period, so that it increases exponentially from an initial to a steady-state frequency. This pattern of accelerating discharge attributed to a Ks conductance has been described in several experimental preparations (Byrne et al., 1979; Getting, 1983; Storm, 1988; Spain et al., 1991a; Marom and Abbott, 1994; Turrigiano et al., 1996).

The initial frequency is approximately constant when a latency preceded the discharge, regardless of the injected current and the initial deinactivation. Numerically, this initial frequency appears to be nonzero at a Hopf bifurcation of the subcritical type (Appendix B). Thus the discharge has a definite nonzero initial frequency. This indicates that there is no correlation between the latency-to-first-spike and the following ISIs. There is a strong correlation between the latency and the first ISI when the Ks conductance is absent, since both are correlated with the injected current. Apart from that, the steady frequency and the initial frequency for immediate discharges follow classic close-to-linear relationship to the injected current.

The pattern of accelerating discharge is complementary to the phenomenon of spike frequency adaptation—that is, a time-dependent decrease in firing frequency during current clamp due to the gradual activation of calcium-gated potassium conductances. These processes can help to set time-varying frequency patterns with gains in the range $\sim$1 to 5 (present results) and $\sim$0.2 to 0.9 (Wang, 1998). However, these regulations rely on very different principles. The former is mainly a subthreshold time-dependent process that evolves following the time constant of inactivation of Ks conductance. The latter is a frequency-dependent

process and has a complex time course related to the time constant of decay of intracellular calcium and the injected current (Wang, 1998).

Effects of Ks Inactivation Under Random Synaptic Stimulation

Latency-to-first-spike under stochastic synaptic stimulation was determined by the structure of the synaptic inputs. Latencies are long for both low stimulation frequencies and strongly deinactivated initial states, and weak input variability. However, early spikes generally occur due to random fluctuations in membrane potential close to the action potential threshold, despite the presence of a strong hyperpolarizing current. Changing the threshold would change the magnitude of the latency effects but would not reduce its variability. Thus the latency cannot be used as a reliable indicator of the initial deinactivation level or the stimulation frequency in these conditions.

Temporal coding can be obtained by integrating a set of presynaptic spike trains that do not exhibit latency-to-first-spike. In this case, the current driving the integrating neuron varies little (approaching current-clamp conditions) since it averages random activity across the presynaptic neurons. Proper temporal ordering of events coded by the control parameters (deinactivation level and stimulation frequency) results from the averaging of small neuronal populations (40 neurons). Although the size of the population depends of the model of synaptic input, it gives a plausible order size. Ensembles of about the same size faithfully encode the spatio temporal characteristics of movement (Georgopoulos et al., 1989; Schwartz, 1993). Population decoding is a general tool for visualizing ongoing neural processing, although the resulting computation need not be explicit (Georgopoulos, 1995). In the present case, latency can be implicitly represented as an ensemble activity or explicitly transmitted to target structures as a discharge.

Synaptically driven model neurons display ramp firing patterns. Firing frequency increases exponentially from an initial to a steady-state frequency with a time constant of $\sim$2.6 s—that is, approximately the time constant of Ks inactivation at mean interspike interval potential. The steady-state frequency is determined by the excitatory input frequency (f_{exc}) and varies linearly with it. The initial frequency increases linearly with f_{exc} and decreases linearly with h_{ini}. Arbitrarily low initial frequencies were obtained *in vivo*, unlike in current-clamp. Therefore, ramp firing patterns with any initial and steady frequency can be produced by the appropriate choice of f_{exc} and h_{ini}. A constant ramp gain (defined by h_{ini}) can be obtained at different output frequencies by varying f_{exc}. Independent control of gain and steady frequency is a feature of *in vivo* conditions but not *in vitro*.

Deinactivation of Ks Conductance

The discharge properties described in this study critically rely on the ease with which the Ks conductance deinactivates. Hence, the question arises whether enough deinactivation can be produced under the electrophysiological conditions encountered *in vivo*. GABAergic synapses have reversal potentials of around -85 mV and give rise to IPSPs that can hyperpolarize the membrane to ~ -75 mV for one second (Avoli, 1986; Howe et al., 1987). According to the deinactivation model of our Ks conductance, these conditions could produce initial deinactivation of up to $\sim$0.5. If we add the constraint that deinactivation is produced by a phasic signal (such as $<$500 ms—that is, short compared to the time course of inactivation), initial deinactivation can be $\sim$0.4. This level of deinactivation is sufficient to have a significant effect on latency-to-first-spike and firing frequency. Thus a transient inhibitory input can act as a signal to "program" latency-to-first-spike or a ramp firing pattern.

Functional Significance

Lashley (1951) suggested that the brain encodes serial order by using a spatial representation. Thus, temporally spaced sensory experiences are translated into spatial patterns of brain activity to construct representations or concepts. The biophysical basis of this transformation may rely on slow intrinsic membrane properties, slow synaptic processes, and short-term plasticity (Buonomano and Merzenich, 1995). The solution capitalizes on the idea that slow variables can carry information about past activity and modulate ongoing spatial interactions within a network. The Ks conductances belong to this family of slow variables and as such may contribute to temporal-to-spatial encoding.

A complementary process is needed to translate spatial patterns of activity into time-varying commands to control sequential actions. The present results suggest that slowly inactivating potassium conductances are

suitable for this task. Since the initial deinactivation level of a Ks conductance determines the future time-varying response of a neuron to an injected current, a spatial distribution of inactivation within a population translates into a distribution of temporal patterns. This output distribution faithfully reflects the temporal order embedded in the spatial input.

Two types of population computation can result from the action of a Ks conductance. First, coding based on the order of spike arrival arises when initial deinactivation results in a discharge with a sizeable latency-to-first-spike. In this case, a transient spatial pattern of inhibition programs the time of the first spike of each neuron. This can result in a temporal version of a "winner-takes-all" process when combined with lateral inhibition (Fukai, 1995). The presence of a Ks conductance makes this process reliable under *in vivo* conditions, which is not the case with "noninactivating" neurons. There is experimental evidence that latency-to-first-spike carries a significant fraction of information on sensory stimulation in behaving animals (Heller et al., 1995; Gawne et al., 1996). More generally, the advantages of coding by the time of spikes have been advocated in numerous studies (Thorpe and Imbert, 1989) and will not be discussed here. The action of a Ks conductance may be relevant to obtain a robust computation based on the time of spikes.

Second, a variety of ramp firing patterns can be elaborated by programming of a neuronal population. Inactivation of the Ks conductance controls the rate of convergence to steady-state discharge behavior in populations of synaptically connected neurons. Since steady state is reached within fractions of the neuron's membrane time constant ($\sim$5 to 10 ms) in most network models of spiking neurons (Hopfield and Herz, 1995; Tsodyks and Sejnowski, 1995; Amit and Brunel, 1997; but see Lukashin and Georgopoulos, 1994; Hansel and Sompolinsky, 1996), the action of the Ks conductance may help explain the slow buildups of neural activity (0.1 to 10 s), which are ubiquitous in behaving animals. Spain et al. (1991a) suggested that the ramp firing patterns recorded during force exertion in sensorimotor neurons could result from a post-hyperpolarization inhibition due to a slow potassium conductance. Cheney and Fetz (1980) described exponentially increasing patterns of discharge frequency in primate corticomotoneurons. We estimate the time constant of increase to be $\sim$200 to 400 ms, which is close to the time constant of Ks inactivation in sensorimotor neurons (Spain et al., 1991b; Foehring and Surmeier, 1993). In the same way, the action of a Ks conductance could underlie the ramp patterns observed before significant events and actions in sensorimotor and cognitive tasks (Apicella et al., 1992; Quintana and Fuster, 1992). These neuronal activities, which signal arrival time, probability of occurrence, or the nature of forthcoming events (Vaadia et al., 1988; Quintana and Fuster, 1992), can be obtained by an appropriate choice of h_{ini} or injected current (stimulation frequency). For example, the time to reach a given frequency level in a population of neurons can be programmed by the intensity of a transient hyperpolarizing current.

Recurrent networks of "slowly inactivating" neurons are unique in their capacity to increase frequency at variable rates. This property is partly due to small variations in initial frequency with stimulation frequency and large variations in steady frequency due to interneuronal interactions. A gradual buildup of discharge through recurrent connections combines with slow inactivation to generate an approximately linear frequency increase over several seconds. The same behavior was observed in a steady-state frequency model over a large range of synaptic conductance (Appendix C). This result indicates that the linearity of frequency increase is not due to a specific choice of a synaptic conductance in relation to the parameters of inactivation but is a general property of the network. The capacity of a network to generate frequency increases at variable rate suggests that the inactivation of a Ks conductance may be relevant for decision-making processes (Hanes and Schall, 1996).

Appendix A. Analytical Study of In Vitro Behavior

We developed an analytical description of the role of Ks inactivation in the discharge behavior of the neuron. Three approximations were made: (1) we replaced the action potential mechanism based on Na and K currents by a threshold θ on the voltage (integrate-and-fire model); (2) since the Ks inactivation gate evolved much more slowly than the membrane voltage ($\tau = 20$ ms) and the Ks activation gate ($\tau_{mKs} = 50$ ms), we assumed that the Ks inactivation gate was the only variable driving the dynamics of the model; (3) we assumed that the mean potential during the delay before the first spike was close to the threshold. These approximations are too rough to obtain an exact fit of the full model. In particular, the activation of Ks is a complex voltage-dependent process that is not well described in this

simplified representation. However, the analytical results provide qualitative information on the parameters of the model. In the following, simplified notations are used: m and h are the Ks gates, m^∞, and h^∞ the voltage-dependence functions, τ_h the time constant of Ks inactivation and $\bar{g}$ the Ks maximal conductance. The initial voltage was always $V_{rest} = -70$ mV and the initial deinactivation level of Ks conductance was h_{ini}.

We determined the time course of membrane potential after a rapid variation due to the charge of the membrane (CdV/dt small compared to other currents) using

$$\bar{g} m_\theta h(t)(V(t) - E_K) + g_{leak}(V(t) - E_{leak}) - I = 0,$$

where $m_\theta = m^\infty(\theta)$. Thus the ramp voltage before the first spike followed

$$V(t) = \frac{\tau(I + \bar{g} m_\theta h(t) E_K) + C E_{leak}}{C + \tau \bar{g} m_\theta h(t)} \tag{1}$$

with

$$h(t) = h_\theta + [h_{ini} - h(\theta)] e^{-t/\tau_{h\theta}}, \tag{2}$$

where $\tau = C/g_{leak}$, $h_\theta = h^\infty(\theta)$, and $\tau_{h\theta} = \tau_h(\theta)$. We determined the time of the first spike T_θ such that $V(T_\theta) = \theta$. From (1), we obtained

$$h(T_\theta) = \frac{\tau I - C(\theta - E_{leak})}{\tau \bar{g} m_\theta (\theta - E_K)}, \tag{3}$$

and we derived from (2)

$$T(\theta) = -\tau_{h\theta} \ln\left(\frac{h(T_\theta) - h_\theta}{h_{ini} - h_\theta}\right) \tag{4}$$

with

$$\begin{aligned} I &< [C(\theta - E_{leak}) + \tau \bar{g} m_\theta (\theta - E_K) h_{ini}]/\tau \\ I &> [C(\theta - E_{leak}) + \tau \bar{g} m_\theta (\theta - E_K) h_\theta]/\tau \end{aligned} \tag{5}$$

corresponding to $0 < T_\theta < \infty$. The threshold θ was adjusted to obtain an appropriate range of delays ($\theta = -53$ mV) and was close to the threshold for action potential in the full model. The equation of the time-of-the-first-spike in the absence of Ks conductance (Lapicque model; Tuckwell, 1988) is shown below for comparison

$$T_\theta = -\tau \ln\left(1 - \frac{C(\theta - E_{leak})}{\tau I}\right). \tag{6}$$

Appendix B. Bifurcation Analysis of Ks Inactivation

We studied the whole model using the qualitative theory of dynamical systems to describe the role of Ks inactivation in the transition between resting potential and repetitive firing. Here the system will be written as

$$\begin{aligned} C\frac{dV}{dt} &+ \bar{g}_{Na} m^3 h (V - E_{Na}) + \bar{g}_K n^4 (V - E_K) \\ &+ \bar{g}_{Ks} m_{Ks} h_{param} (V - E_K) + g_{leak}(V - E_{leak}) - I = 0 \end{aligned}$$

$$\frac{d\phi}{dt} = \frac{\phi^\infty(V) - \phi}{\tau_\phi(V)} \quad \phi = m, h, n, m_{Ks}.$$

The bifurcation behavior of the system was determined as the bifurcation parameter (h_{param}) was varied while other parameters and I remained constant. The stationary solution corresponding to the resting potential (V_{RP}) was obtained for each input current by solving

$$\begin{aligned} &\bar{g}_{Na} m(V_{RP})^3 h(V_{RP})(V_{RP} - E_{Na}) + \bar{g}_K n(V_{RP})^4 \\ &\quad \times (V_{RP} - E_K) + \bar{g}_{Ks} m(V_{RP}) h_{param} (V_{RP} - E_K) \\ &\quad + g_{leak}(V_{RP} - E_{leak}) - I = 0. \end{aligned}$$

The Jacobian matrix of the system was computed, and its eigenvalues determined the stability of the stationary solution. Similar results were observed at all input currents tested.

An asymptotically stable stationary solution was found for values of $h_{param} > h_{RP}$, corresponding to resting potentials of ~ -75 mV ($h_{param} = 1$) to ~ -50 mV ($h_{param} = h_{RP}$). At $h_{param} = h_{RP}$, the real part of two conjugate complex eigenvalues crossed the imaginary axis, becoming positive as h_{Param} was decreased. This indicated that an Andronov-Hopf bifurcation occurred at this point (Kuznetsov, 1995). Numerical simulations showed the appearance of unstable oscillations around the resting potential for $h_{RP} < h_{param} < h_{osc}$, which strongly suggested that the bifurcation was subcritical. Large amplitude stable oscillations (repetitive spiking) were found for $h_{param} < h_{osc}$. Their minimal frequency, measured at $h_{param} = h_{osc}$, was nonzero. Unstable and stable oscillations coexisted with the stable resting potential in a small region ($h_{RP} < h_{param} < h_{osc}$), resulting in a domain of bistability. Finally, these results strongly indicate that the bifurcation can be classified as a subcritical Andronov-Hopf bifurcation at

$h_{param} = h_{RP}$, accompanied by a saddle-node bifurcation of limit cycle at $h_{param} = h_{osc}$ (turning point; Iooss and Joseph, 1990).

Appendix C. Analytical Study of Recurrent Network Behavior

We explored the behavior of the spiking recurrent network in a simplified model based on frequency changes. We considered a mean field approximation of network operations. We assumed that synaptic interactions were much faster than Ks inactivation. We wrote

$$f(t) = F(I + gf(t), h(t)),$$

where f is the mean network frequency, I is a feedforward current, g represents synaptic coupling between neurons, and

$$F(i, h) = \alpha + (\beta - \gamma i) \ln h$$

is the steady frequency curve obtained by curve fitting from Fig. 8A ($\alpha = -3$, $\beta = 40.4$, $\gamma = 6.1$). We obtained

$$f(t) = \frac{\alpha + (\beta - \gamma I) \ln h(t)}{1 + \gamma g \ln h(t)}, \tag{7}$$

where the inactivation gate h followed

$$h(t) = h_\infty + (h_{ini} - h_\infty) \exp(-t/\tau_h),$$

where h_∞ is the steady-state value of h ($h_\infty = 0.08$). We calculated a first-order approximation of Eq. (7) for $t \ll \tau_h$ and $\gamma g \ll 1$

$$f(t) = st + f_0 \tag{8}$$

with

$$f_0 = \frac{\alpha + (\beta - \gamma I) \ln h_{ini}}{1 + \gamma g \ln h_{ini}}$$

and

$$s = \frac{(h_{ini} - h_\infty)(\gamma I + \gamma g f_0 \beta)}{h_{ini} \tau_h (1 + \gamma g \ln h_{ini})}. \tag{9}$$

We verified the validity of Eq. (8) numerically. The frequency deviated from the theoretical frequency (7) by less than 10% for $t \leq \tau_h$ for a wide range of I, h_{ini}, and g. Equation (9) gives the slope of the frequency increase as a function of paramaters of the model. In particular, it shows that the slope increases linearly with I and nonlinearly with g (note that $\ln(h_{ini}) < 0$).

Acknowledgments

We thank S. Charpier, J.M. Deniau, and L. Borg-Graham for fruitful discussions and O. Parkes and C. Langram for revising our English. This work was supported in part by a grant from GIS-Cogniscience (E.G).

References

Amit D, Brunel N (1997) Dynamics of a recurrent network of spiking neurons before and following learning. *Network: Comput. Neural Syst.* 8:373–404.

Apicella P, Scarnati E, Ljungberg T, Schultz W (1992) Neuronal activity in monkey striatum related to the expectation of predictable environmental events. *J. Neurophysiol.* 68:945–960.

Avoli M (1986) Inhibitory potentials in neurons of the deep layers of the *in vitro* neocortical slice. *Brain Res.* 370:165–170.

Bargas J, Galarraga E (1995) Ion channels: Keys to neuronal specialization. In: M Arbib, ed. The Handbook of Brain Theory and Neural Networks. MIT Press, Cambridge, pp. 496–501.

Bargas J, Galarraga E, Aceves J (1989) An early outward conductance modulates the firing latency and frequency of neostriatal neurons of the rat brain. *Exp. Brain Res.* 75:146–156.

Barkai E, Bergman R, Horwitz G, Hasselmo M (1994) Modulation of associative memory function in a biophysical simulation of rat piriform cortex. *J. Neurophysiol.* 72(2):659–677.

Booth V, Rinzel J, Kiehn O (1997) Compartmental model of vertebrate motoneurons for Ca^{2+}-dependent spiking and plateau potentials under pharmacological treatment. *J. Neurophysiol.* 78(6):3371–3385.

Buonomano D, Merzenich M (1995) Temporal information transformed into a spatial code by a neural network with realistic properties. *Science* 267:1028–1030.

Byrne J (1980) Quantitative aspects of ionic conductance mechanisms contributing to firing pattern of motor cells mediating inking behaviour in Aplysia Californica. *J. Neurophysiol.* 43:651–668.

Byrne J, Shapiro E, Dieringer N, Koester J (1979) Biophysical mechanisms contributing to inking behavior in Aplysia. *J. Neurophysiol.* 42:1233–1250.

Camperi M, Wang X-J (1998) A model of visuospatial working memory in prefrontal cortex: Recurrent network and cellular bistability. *J. Comput. Neurosci.* 5(4):383–405.

Cartling B (1993) Control of the complexity of associative memory dynamics by neuronal adaptation. *Int. J. Neural Syst.* 4:129–141.

Cartling B (1997) Control of computational dynamics of coupled integrate-and-fire neurons. *Biol. Cybern.* 76(5):383–395.

Cheney P, Fetz E (1980) Functional classes of primate corticomotoneuronal cells and their relation to active force. *J. Neurophysiol.* 44:773–791.

Delord B, Klaassen A, Burnod Y, Costalat R, Guigon E (1997) Bistable behaviour in a neocortical neurone model. *NeuroReport* 8(4):1019–1023.

Deuchars J, Thomson A (1995) Single axon fast inhibitory postsynaptic potentials elicited by a sparsely spiny interneuron in rat neocortex. *Neuroscience* 65:935–942.

Foehring R, Surmeier D (1993) Voltage-gated potassium currents in acutely dissociated rat cortical neurons. *J. Neurophysiol.* 70:51–63.

Fukai T (1995) A model cortical circuit for the storage of temporal sequences. *Biol. Cybern.* 72(4):321–328.

Gabel L, Nisenbaum E (1998) Biophysical characterization and functional consequences of a slowly inactivating potassium current in neostriatal neurons. *J. Neurophysiol.* 79(4):1989–2002.

Gawne T, Kjaer T, Hertz J, Richmond B (1996) Adjacent visual cortical complex cells share about 20% of their stimulus-related information. *Cereb. Cortex* 6(3):482–489.

Georgopoulos A (1995) Current issues in directional motor control. *Trends Neurosci.* 18(11):506–510.

Georgopoulos A, Crutcher M, Schwartz A (1989) Cognitive spatial-motor processes. 3. Motor cortical prediction of movement direction during an instructed delay period. *Exp. Brain Res.* 75:183–194.

Getting P (1983) Mechanisms of pattern generation underlying swimming in Tritonia. III. Intrinsic and synaptic mechanisms for delayed excitation. *J. Neurophysiol.* 49:1036–1050.

Golomb D, Amitai Y (1997) Propagating neuronal discharges in neocortical slices: Computational and experimental study. *J. Neurophysiol.* 78:1199–1211.

Guigon E, Dorizzi B, Burnod Y, Schultz W (1995) Neural correlates of learning in the prefrontal cortex of the monkey: A predictive model. *Cereb. Cortex* 5:135–147.

Gutfreund Y, Yarom Y, Segev I (1995) Subthreshold oscillations and resonant frequency in guinea-pig cortical neurons: Physiology and modelling. *J. Physiol. (Lond.)* 483(3):621–640.

Hammond C, Crépel F (1992) Evidence for a slowly inactivating K^+ current in prefrontal cortical cells. *Eur. J. Neurosci.* 4:1087–1092.

Hanes D, Schall J (1996) Neural control of voluntary movement initiation. *Science* 274:427–430.

Hansel D, Sompolinsky H (1996) Chaos and synchrony in a model of a hypercolumn in visual cortex. *J. Comput. Neurosci.* 3:7–34.

Harris-Warrick R, Marder E (1991) Modulation of neural networks for behavior. *Ann. Rev. Neurosci.* 14:39–57.

Heller J, Hertz J, Kjaer T, Richmond B (1995) Information flow and temporal coding in primate pattern vision. *J. Comput. Neurosci.* 2(3):175–193.

Hopfield J, Herz A (1995) Rapid local synchronization of action potentials: Toward computation with coupled integrate-and-fire neurons. *Proc. Natl. Acad. Sci. USA* 92(15):6655–6662.

Howe J, Sutor B, Zieglgansberger W (1987) Baclofen reduces postsynaptic potentials of rat cortical neurons by an action other than its hyperpolarizing action. *J. Physiol. (Lond.)* 384:539–569.

Huguenard J, McCormick D (1992) Simulation of the current involved in rhythmic oscillations in thalamic relay neurons. *J. Neurophysiol.* 68:1373–1383.

Huguenard J, Prince D (1991) Slow inactivation of a TEA-sensitive K current in acutely isolated rat thalamic relay neurons. *J. Neurophysiol.* 66:1316–1328.

Iooss G, Joseph D (1990) Elementary Stability and Bifurcation Theory (2nd ed.). Springer-Verlag, New York.

Kiehn O (1991) Plateau potentials and active integration in the final common pathway for motor behavior. *Trends Neurosci.* 14:68–73.

Komatsu Y, Nakajima S, Toyama K, Fetz E (1988) Intracortical connectivity revealed by spike-triggered averaging in slice preparations of cat visual cortex. *Brain Res.* 442:359–362.

Kuznetsov Y (1995) Elements of Applied Bifurcation Theory: Applied Mathematical Sciences, 112. Springer-Verlag, New York.

Lanthorn T, Storm J, Andersen P (1984) Current-to-frequency transduction in CA1 hippocampal pyramidal cells: Slow prepotentials dominate the primary range firing. *Exp. Brain Res.* 53:431–443.

Lashley K (1951) The problem of serial order in behavior. In: L Jeffres, ed. Cerebral Mechanisms of Behavior. Wiley, New York, pp. 112–136.

LeMasson G, Marder E, Abbott L (1993) Activity-dependent regulation of conductances in model neurons. *Science* 259:1915–1918.

Lisberger S, Sejnowski T (1992) Motor learning in a recurrent network model based on the vestibulo-ocular reflex. *Nature* 360:159–161.

Llinás R (1988) The Intrinsic electrophysiological properties of mammalian neurons: Insights into central nervous system function. *Science* 242:1654–1663.

Lukashin A, Georgopoulos A (1994) A neural network for coding trajectories by time series of neuronal population vectors. *Neural Comput.* 6:19–28.

Lüthi A, Gahwiler B, Gerber U (1996) A slowly inactivating potassium current in CA3 pyramidal cells of rat hippocampus *in vitro*. *J. Neurosci.* 16(2):586–594.

Lytton W, Sejnowski T (1991) Simulations of cortical pyramidal neurons synchronized by inhibitory interneurons. *J. Neurophysiol.* 66:1059–1079.

Marder E, Abbott L, Turrigiano G, Liu Z, Golowasch J (1996) Memory from the dynamics of intrinsic membrane currents. *Proc. Natl. Acad. Sci. USA* 93(24):13481–13486.

Marom S, Abbott L (1994) Modeling state-dependent inactivation of membrane currents. *Biophys. J.* 67:515–520.

Marom S, Levitan I (1994) State-dependent inactivation of the Kv3 potassium channel. *Biophys. J.* 67:579–589.

Mason A, Nicoll A, Stratford K (1991) Synaptic transmission between individual pyramidal neurons of the rat visual cortex *in vitro*. *J. Neurosci.* 11:72–84.

McCormick D (1991) Functional properties of a slowly inactivating potassium current in guinea pig dorsal lateral geniculate relay neurons. *J. Neurophysiol.* 66:1176–1189.

Nicoll A, Blakemore C (1993) Single-fibre EPSPs in layer 5 of rat visual cortex *in vitro*. *NeuroReport* 4:167–170.

Nisenbaum E, Xu Z, Wilson C (1994) Contribution of a slowly-inactivating potassium current to the transition to firing of neostriatal spiny projection neurons. *J. Neurophysiol.* 71:1174–1189.

Peters A (1987) Number of neurons and synapses in primary visual cortex. In: A Peters, E Jones, eds. Cerebral Cortex, Vol. 6: Further Aspects of Cortical Function, Including Hippocampus. Plenum Press, New York, pp. 267–294.

Quintana J, Fuster J (1992) Mnemonic and predictive functions of cortical neurons in a memory task. *NeuroReport* 3:721–724.

Rush M, Rinzel J (1995) The potassium A-current, low firing rates and rebound excitation in Hodgkin-Huxley models. *Bull. Math. Biol.* 57:899–929.

Schwartz A (1993) Motor cortical activity during drawing movements: Population representation during sinusoidal tracing. *J. Neurophysiol.* 70:28–36.

Shadlen M, Newsome W (1994) Noise, neural codes and cortical organization. *Curr. Opin. Neurobiol.* 4(4):569–579.

Silva L, Amitai Y, Connors B (1991) Intrinsic oscillations of neocortex generated by layer 5 pyramidal neurons. *Science* 251:432–435.

Softky W, Koch C (1993) The highly irregular firing of cortical cells is inconsistent with temporal integration of random EPSPs. *J. Neurosci.* 13:334–350.

Spain W, Schwindt P, Crill W (1991a) Post-inhibitory excitation and inhibition of layer V pyramidal neurones from cat sensorimotor cortex. *J. Physiol. (Lond.)* 434:609–626.

Spain W, Schwindt P, Crill W (1991b) Two transient potassium currents in layer V pyramidal neurones from cat sensorimotor cortex. *J. Physiol. (Lond.)* 434:591–607.

Stevens C, Zador A (1998) Input synchrony and the irregular firing of cortical neurons. *Nat. Neurosci.* 1(3):210–217.

Storm J (1988) Temporal integration by a slowly inactivating K^+ current in hippocampal neurons. *Nature* 336:379–381.

Surmeier D, Stefani A, Foehring R, Kitai S (1991) Developmental regulation of a slowly-inactivating potassium conductance in rat neostriatal neurons. *Neurosci. Lett.* 122:41–46.

Thomson A, West D, Hahn J, Deuchars J (1996) Single axon IPSPs elicited in pyramidal cells by three classes of interneurones in slices of rat neocortex. *J. Physiol. (Lond.)* 496(1):81–102.

Thorpe S, Imbert M (1989) Biological constraints on connectionist modelling. In: R Pfeifer, Z Schreter, F Fogelman-Soulié, L Steels, eds. Connectionism in Perspective. Elsevier Science, Amsterdam, pp. 63–92.

Tsodyks M, Sejnowski T (1995) Rapid state switching in balanced cortical network model. *Network: Comput. Neural Syst.* 6:111–124.

Tuckwell H (1988) Introduction to Theoretical Neurobiology, Vol 1: Linear Cable Theory and Dendritic Structure. Cambridge University Press, Cambridge.

Turrigiano G, Marder E, Abbott L (1996) Cellular short-term memory from a slow potassium conductance. *J. Neurophysiol.* 75(2):963–966.

Vaadia E, Kurata K, Wise S (1988) Neuronal activity preceding directional and nondirectional cues in the premotor cortex of rhesus monkeys. *Somatosens. Mot. Res.* 6:207–230.

Wang H, McKinnon D (1995) Potassium currents in rat prevertebral and paravertebral sympathetic neurons: Control of firing properties. *J. Physiol. (Lond.)* 485:319–335.

Wang X-J (1993) Ionic basis for intrinsic 40 Hz neuronal oscillations. *NeuroReport* 5:221–224.

Wang X-J (1998) Calcium coding and adaptive temporal computation in cortical pyramidal neurons (correction in 80(2):U9–U9). *J. Neurophysiol.* 79(3):1549–1566.

Wilson C (1995) Dynamic modification of dendritic cable properties and synaptic transmission by voltage-gated potassium channels. *J. Comput. Neurosci.* 2:91–115.